

Optimal design and cost analysis of single-axis tracking photovoltaic power plants

A. Barbón^a, V. Carreira-Fontao^b, L. Bayón^{c,*}, C.A. Silva^d

^a Department of Electrical Engineering, University of Oviedo, Spain

^b Polytechnic School of Engineering of Gijón, University of Oviedo, Spain

^c Department of Mathematics, University of Oviedo, Spain

^d Center for Innovation, Technology and Policy Research –IN+, Instituto Superior Técnico, University of Lisbon, Portugal

ARTICLE INFO

Keywords:

Single-axis tracker
Optimisation algorithm
Normal tracking mode
Backtracking mode
Energy gain
Analysis cost

ABSTRACT

The increasing penetration of photovoltaic technology in the electricity market requires the development of a methodology that facilitates the optimisation of photovoltaic plants with single-axis trackers. This paper presents an optimisation methodology that takes into account the most important design variables of single-axis photovoltaic plants, including irregular land shape, size and configuration of the mounting system, row spacing, and operating periods (for backtracking mode, limited range of motion, and normal tracking mode). Equations for the determination of the optimal row spacing and operating periods have been developed and is presented in detail. A packing algorithm that takes into account the irregular land shape and the possible configurations of the mounting systems is also presented. The objective function is the total area of the photovoltaic field and the optimisation is performed by a packing algorithm. As the economic aspect of energy generation also plays a key role in decision-making, the levelised cost of energy has been used to assess the economic viability of the optimal layout of the mounting systems. The results show that the proposed methodology and packing algorithm are able to optimise the photovoltaic plant with single-axis solar tracking and provide reliable results after a reasonable computation time. The methodology was demonstrated in detail for a Spanish photovoltaic plant (Granjera photovoltaic power plant), including the optimal layout of the mounting systems and the cost analysis for this layout. The optimal layout of the mounting systems could increase the amount of energy captured by 91.18% in relation to the current of Granjera photovoltaic power plant. The mounting system configuration used in the optimal layout is the one with the best levelised cost of energy efficiency, 1.09. The presented optimisation methodology can be utilised to facilitate the optimal design of commercial photovoltaic plants with single-axis trackers. Therefore, questions such as: what is the optimal distribution of mounting systems?, how much energy will this distribution produce?, and at what cost will it produce it?, can be answered by using the proposed methodology.

1. Introduction

The growing emphasis of developed countries on reducing environmental pollution caused by fossil fuels highlights the reliance on renewable energy worldwide [1]. For this reason, many researchers have focused on investigating the application of renewable energy sources, such as solar energy Photovoltaic systems [2], thermosolar systems [3] or wind energy [4].

Photovoltaic (PV) systems are growing rapidly and are expected to play an important role in global power generation. The total installed capacity was around 754 (GW) at the end of 2020 [5]. To compare the economic viability of various energy sources such as solar energy, wind

energy, hydropower, natural gas, the levelised cost of energy (LCOE) is often used [3,6]. LCOE, which indicates the average cost of a power plant to generate energy considering investment and operation costs, can also be used to compare different PV plant configurations [2]. This parameter can be used to demonstrate the cost reduction of PV plants. For example, the weighted average LCOE in 2018 was 0.085 (USD/kWh), and is estimated to be between 0.02 and 0.08 (USD/kWh) by 2030 and between 0.014 and 0.05 (USD/kWh) by 2050 [7].

The growth in PV systems is due to several factors. The most important of these is the substantial reduction in PV module costs [8]. In 2017, the International Renewable Energy Agency (IRENA) presented

* Corresponding author.

E-mail addresses: barbon@uniovi.es (A. Barbón), carreirafontao@gmail.com (V. Carreira-Fontao), bayon@uniovi.es (L. Bayón), carlos.santos.silva@tecnico.ulisboa.pt (C.A. Silva).

<https://doi.org/10.1016/j.renene.2023.04.110>

Received 23 December 2022; Received in revised form 4 April 2023; Accepted 22 April 2023

Available online 2 May 2023

0960-1481/© 2023 The Author(s). Published by Elsevier Ltd. This is an open access article under the CC BY-NC license (<http://creativecommons.org/licenses/by-nc/4.0/>).

Nomenclature table

A_{TPV}	Total photovoltaic modules area (m ²)
C_{CS}	Unit cost of the control system (€/unit)
C_{cb}	Costs of the cable (€)
C_{EM}	Unit cost of the electric motor (€/unit)
C_e	Exposure factor
C_i	Initial investment cost (€)
C_{inv}	Unit cost of the inverter (€/unit)
C_L	Cost of the land area (€)
C_M	Costs of the monitoring system (€)
C_{MS}	Unit cost of the mounting structure (€/unit)
C_{OM}	Cost of operation and maintenance (€)
C_p	Pressure coefficient
C_{PD}	Costs of the protection devices (€)
C_{prob}	Probability factor
C_{PV}	Unit cost of a PV module (€/unit)
C_T	Costs of the transformer (€)
C_{Ti}	Total cost of the project (€)
d	Distance $E - W$ between two adjacent mounting systems (m)
d_r	Annual degradation rate
d_{min}	Minimum distance $E - W$ between two adjacent mounting systems (m)
d_{st}	Standard distance $E - W$ between two adjacent mounting systems (m)
E_i	Availability of solar resource at the i th year (kWh)
E_{TPV}	Total energy on the photovoltaic modules (MWh)
e_l	Distance $N - S$ between two adjacent mounting systems (m)
e_s	Minimum distance on the ground (m)
e_t	Pitch (m)
GCR	Ground coverage ratio (dimensionless)
\mathbb{H}_t	Adjusted total irradiation on a tilted surface (Wh/m ²)
k	Parameter that depend on the terrain
I	Lifetime of the project (years)
\mathbb{I}_{bh}	Adjusted beam irradiance on a horizontal surface (W/m ²)
\mathbb{I}_{dh}	Adjusted diffuse irradiance on a horizontal surface (W/m ²)
\mathbb{I}_t	Adjusted total irradiance on a horizontal surface (W/m ²)
L	Length of the mounting system (m)
L_e	Parameter that depend on the terrain
L_{PV}	Length of the photovoltaic modules (m)
$LCOE$ efficiency	Ratio between the $LCOEs$ rack configurations
N_{CS}	Total number of control systems
N_{EM}	Total number of electric motors
N_{inv}	Total number of inverters
N_{MS}	Total number of mounting structures
N_{PV}	Number of photovoltaic modules
n	Ordinal of the day (day)

\bar{P}	Available land area (m ²)
p	Height of the column (m)
q_b	Basic velocity pressure (kN/m ²)
q_e	Static pressure (kN/m ²)
q_{PV}	Load due to the weight of the PV modules (kN/m ²)
r	Discount rate for i th year
S	Projection the L on the horizontal plane (m)
S_i	Total electrical energy output at the i th year (kWh)
S_L	Snow load (kg)
T	Solar time (h)
T_R	Sunrise solar time (h)
T_S	Sunset solar time (h)
T_{b1}	End of the backtracking mode (h)
T_{b2}	Start of the backtracking mode (h)
$T_{\beta 1}$	Start of the normal tracking mode (h)
$T_{\beta 2}$	End of the normal tracking mode (h)
v_b	Basic wind velocity (m/s)
W	Width of the mounting system (m)
W_{ePV}	Weight of the PV module (kg)
W_{eS}	Weight of the structure (kg)
W_L	Wind load (kg)
W_{PV}	Width of the photovoltaic modules (m)
z	Height on the ground (m)
α_S	Height angle of the Sun (°)
β	Tilt angle of photovoltaic module (°)
β_B	Backtracking angle (°)
β_{max}	Limited range of motion angle (°)
β_{st}	Standard tilt angle of photovoltaic module (°)
γ	Azimuth angle of photovoltaic module (°)
γ_S	Azimuth of the Sun (°)
δ	Solar declination (°)
η	Performance factor
θ_c	Backtracking correction angle (°)
θ_i	Incidence angle (°)
θ_t	Transversal angle (°)
θ_{tb}	Backtracking angle (°)
θ_{tst}	Standard transversal angle (°)
θ_z	Zenith angle of the Sun (°)
λ	Latitude angle (°)
ρ	Air density (Kg/m ³)
ρ_g	Ground reflectance (dimensionless)
ω	Hour angle (°)

a report in which it predicted a 60% drop in the PV module cost over the next 10 years [9]. The current price of 0.266 (USD/W_p) [10] allows large-scale PV plants to be competitive from the point of view

of this component. While PV modules have come down in price, the other components of the system (mounting systems, inverters, cables, power protection systems, measuring equipment, system monitoring, etc.) have increased in cost, with the PV module mounting system accounting for a substantial part [11]. Therefore, a study on mounting systems is needed to increase the energy and consequentiality the economic efficiency of PV systems.

The mounting systems can be classified into two categories: with and without solar tracking system. As the movement of the Sun in the sky throughout the day is continuous, it is obvious that the most efficient PV module mounting system is one that is equipped with solar tracking [2]. Therefore, in order to maximise the amount of solar irradiance incident on the PV modules, solar tracking systems

(*STS*) have been developed to align the *PV* modules with the Sun. Applications of *STS*s are various, such as large-scale *PV* plants [12], *PV* greenhouses [13], and *PV* pump storage systems [14]. This study focuses on large-scale *PV* plants. However, these advances are not always properly applied to *PV* plant design and/or operation, and, consequently, the optimal development that these advances require for *PV* plants has not yet been achieved.

*STS*s are generally categorised according to the number of rotational motions [2]: dual-axis tracking (with two axes of rotation) and single-axis tracking (with one axis of rotation and different orientations). Dual-axis tracking allows the *PV* module to orientate towards any direction of the celestial sphere. According to the orientation of the rotation axis, single-axis tracking can have the following configurations [2]: (i) Single-axis tracker configuration with horizontal North–South axis and East–West tracking (rotating around a horizontal axis aligned with the North–South axis), and (ii) Single-axis tracker configuration with horizontal East–West axis and North–South tracking (rotating around a horizontal axis aligned with the East–West axis). Other arrangements of the axis of rotation are possible from a theoretical point of view, but not from a practical point of view [15].

Obviously, dual-axis tracker systems show the best results. In [2], solar resources were analysed for all types of tracking systems at 39 sites in the northern hemisphere covering a wide range of latitudes. Dual-axis tracker systems can increase electricity generation compared to single-axis tracker configuration with horizontal North–South axis and East–West tracking from 2.59% up to 15.88%, and compared to single-axis tracker configuration with horizontal East–West axis and North–South tracking from 12.62 up to 21.95%. Because the single-axis tracker configuration with horizontal North–South axis and East–West tracking produces more energy than the single-axis tracker configuration with horizontal East–West axis and North–South tracking, the former will be the subject of this study. Furthermore, to simplify its name, it will be called horizontal single-axis tracker [15].

For large-scale *PV* plants, other factors have to be taken into account, such as initial investment costs, operation and maintenance cost, available land area, soil conditions, and wind loads [11,16,17]. A dual-axis tracker typically represents a 20–25% increase in average installation costs compared to a horizontal single-axis tracking configuration, assuming the large-scale *PV* plant is of the same size [15]. Martín et al. [16] evaluated six large-scale *PV* plants in Spain and concluded that the complexity of the dual-axis tracking system is underestimated from an operation and maintenance point of view. On the other hand, an economic study using the so-called levelised cost of electricity indicator was presented in [2,17]. Both works concluded that horizontal single-axis tracking configuration is more advantageous than dual-axis tracking system. In practice, the horizontal single-axis tracking system is the most commonly used [15]. Because to the high utilisation of the horizontal single-axis tracking system in large-scale *PV* plants, the optimisation of its performance is a task of great importance.

Due to the large number of variables that have to be taken into account in the design of a *PV* plant, this task is complex [18]. These variables can be grouped as: variables related to the land (available land area, land shape, land orientation, land inclination), variables related to climatic conditions (geographical location, local weather conditions), variables related to the technology used (mounting system configuration with and without solar tracking system, choice of normal tracking strategy and backtracking strategy for solar tracking mounting systems, *PV* module, inverter, etc.), variables related to the operation of the plant (environment favourable to soiling of *PV* modules, availability of water for cleaning the *PV* modules), and variables related to nearby infrastructure (good accessibility, availability of a power grid and the accessibility to it, etc.). Several disciplines have to work together to achieve a good design. Therefore, the designer must select the components of the *PV* system, such as the layout of the mounting systems, the mounting systems configuration, the number of

mounting systems, the model of the *PV* modules, the number and type of inverters, etc.

As discussed above, the optimisation strategy for a *PV* plant can depend on a large number of variables. Therefore, several methodologies have been proposed depending on the final objective.

Alves et al. [19] presented the design optimisation of utility-scale single-axis tracking *PV* plants, using evaluation metrics that take into account both the energy yield and the total energy production efficiency of the *PV* plant. For this purpose, they used 26,700 simulations of different combinations of the constructive aspects of a base *PV* plant as well as different modules used. Two mounting system topologies were evaluated: (i) fixed tilt angle and (ii) horizontal single-axis tracker. However, this work does not consider other conditions that depend on the mounting system configuration, such as the periods of operation or the inter-row spacing design.

János and Gróf [20] described a method for the simultaneous optimisation of 10 design parameters of a photovoltaic plant, including electrical parameters (*PV* module power, series *PV* modules number, parallel strings number, inverters number, *DC* voltage drop, *AC* voltage drop, cable losses), and topological parameters (*PV* module tilt angle, *PV* module orientation, distance between rows, support structure dimensions). The main differences with the present study is that it uses mounting systems with a fixed tilt angle. Furthermore, the layout of the mounting system and the landscape have not been taken into account.

Bayón et al. [21] presented the optimal distribution of mounting systems with a fixed tilt angle on flat roofs of urban building so that the total absorbed energy is maximised. The main differences between this work and the study presented here is that it uses photovoltaic systems without solar tracking system and the shape of the surface is regular. Therefore, the algorithm used is less complex than the one presented here, among other reasons, because the shadow study is more complex as the *PV* modules have movement.

As the availability of rooftop space has been identified as an important limiting factor in the installation of *PV* systems, the authors [22] presented an algorithm that optimises the deployment of *PV* modules on irregular shaped rooftops. In addition to using mounting systems without solar tracking system, the space available is limited. These are the two major differences with the work presented here. Therefore, the algorithm used is less complex than the one presented here. The movement of the photovoltaic modules complicates the study of shadows.

Barbón et al. [11] determined the optimal distribution of mounting system with a fixed tilt angle on irregular land shapes. To do this, they used a packing algorithm. Different mounting system configurations and tilt angles are incorporated in the study to take into account the irregular land shape. There are very important differences with respect to the study presented here. As the current study uses mounting systems with horizontal single-axis tracker configuration, the shading study between *PV* modules is different, and the determination of the solar tracking algorithm was not the subject of the previous study.

Tahir et al. [23] presented a worldwide study, using a novel approach to decouple energy performance from cost considerations, by parameterising the *LCOE* formula in terms of “land-related cost” and “module-related cost” to demonstrate that an interaction of these parameters defines the optimal design of *PV* plants with bifacial modules. This study does not take into account the land shape and different mounting system configurations, which are key parameters in optimising the layout of mounting systems in a *PV* plant.

Aronescu and Appelbaum [24] optimised the solar field of *PV* plants with the following decision variables: *PV* module tilt angle, height of rows, rows number, distance between rows, series *PV* modules number, parallel strings number, and the dimensions of the field’s total area. The main differences with the present study is that it uses mounting systems with a fixed tilt angle without taking into account the possible configurations of the mounting system, and regular shapes

of the land, which makes the study presented here totally different and more complex.

Despite the importance of the issue, as this kind of research helps decision-making on *PV* plant design, only a few papers deal with the optimisation of large-scale *PV* plant design. And none of them take into account the land shape, the use of single-axis trackers, and the possible configurations of mounting systems. To do this, it is necessary to identify the factors that can help improve the performance of a *PV* plant with single-axis solar tracking, such as:

- (i) Available land area. As a consequence of low *PV* module prices and high land costs, it is necessary to optimise the layout of *PV* modules on land to maximise the return on land investment [25]. In this sense, the aim is to achieve the maximum energy production per available land area, rather than the optimum energy production per peak power [11]. Ong et al. [26] conducted a comprehensive analysis of almost 200 *PV* plants in the United States. They distinguish between the total and the direct land area. The total land area comprises all the land enclosed by the site boundary. On the other hand, the land occupied by *PV* modules, buildings (offices and sanitary rooms, low voltage/medium voltage station, medium voltage/high voltage station, communications) and access roads, is referred to as direct land area. However, there is not much data in the literature on the direct area occupied by *PV* modules in *PV* plants [27]. This is very important, as this surface can be related to the installed *PV* module area, and therefore, it can be associated with the generated *PV* energy [27]. Therefore, during the design phase of a *PV* plant, it is necessary to analyse the direct surface area occupied by the *PV* modules. However, there are few studies available in the literature on this parameter. If the *PV* field is not physically constrained, it simplifies the problem a lot, but this is not the situation in most cases.
- (ii) Land shape. The shape of the land plays a crucial role in the layout of the mounting systems in large-scale *PV* plants. The basic shape of the land is rectangular or a combination of this shape. However, this shape is not the most common. The usual shape of large-scale *PV* plants is the irregular shape. Several studies have shown increased complexity in the design of *PV* systems due to the irregular land shape [11].
- (iii) Self-shading of *PV* modules. Shading in certain modules caused by nearby module rows is called self-shading. Self-shading plays a significant role in the design of the solar tracking algorithm as it affects the total energy generated [25]. This is because the shaded cells do not receive the beam component of the solar irradiance and, consequently, the solar irradiance levels captured for partially shaded *PV* modules are considerably reduced. Another negative effect of self-shading on the *PV* module, which can cause it to deteriorate, is the appearance of hot spots in the shaded cell [28]. The shaded cell becomes a resistor that consumes the energy of neighbouring cells in its own string, increasing the cell temperature and producing hot spots. Therefore, estimating the hours of the day when shading losses occur is essential. However, the problem is very complex, since in addition to the solar geometry, it is affected by many variables related to the design of the *PV* plant, such as the spacing between rows of *PV* modules, the mounting system configuration, the land shape, etc. Therefore, the effect of inter-module shading on energy conversion in *PV* plants has been the subject of many studies [29,30]. In the central hours of the day there can also be energy losses due to self-shading. These losses are regulated by various legislations [31]. In this sense, this paper presents a calculation process to determine the minimum distance between rows of modules of a *PV* plant with single-axis solar tracking that minimises the effect of shadows between *PV* modules. These energy losses are more difficult to avoid in the early hours of the day. For this purpose, a suitable solar tracking algorithm called backtracking can be used.

- (iv) Operational periods of solar tracking. The determination of the solar tracking operating periods are essential for the design of the solar tracking algorithm that maximises the effective annual incident energy on the *PV* modules. These periods of operation can be classified as follows: backtracking mode, limited range of motion, and normal tracking mode. The analysis of these periods of operation is one of the objectives of this study.
- (v) *PV* module mounting system configuration. In this paper, *PV* plants with horizontal single-axis tracking are analysed. This tracking system supports several configurations of *PV* modules such as 1 V and 2 V. It is common for several configurations of different sizes to be used in the same *PV* plant [15]. They have the same width, but different lengths, i.e. larger size configuration and smaller size configuration. For example, 1 V × 56 (larger size) and 1 V × 28 (smaller size). As it has been shown in other studies [11,21], these configurations have a strong influence on the energy generated on a given surface.

Taking all these factors into account in the design of large-scale *PV* plants is complex due to the large number of *PV* modules involved. In this line of research, this study aims to optimise the distribution of single-axis solar trackers in large-scale *PV* plants that optimises the capture of solar irradiance by *PV* modules and, consequently, to maximise the conversion of electrical energy. In order to achieve this objective, this paper proposes the following methodology: (i) Inter-row spacing design; (ii) Determination of operating periods of the *PV* system; (iii) Optimal number of solar trackers; and (iv) Determination of the effective annual incident energy on *PV* modules.

Faced with so many design options, the aim of this paper is to show a methodology for finding the optimal layout of single-axis solar trackers in large-scale *PV* plants. In order to illustrate the methodology, a study of a large-scale photovoltaic plant located in Spain is presented in detail. Compared to previous reviews on this issue, the main contributions of this paper can be summarised as follows:

- (i) A detailed analysis of the design of the inter-row spacing and operating periods of the *PV* system.
- (ii) The algorithm presented in this paper for each mounting system configuration and size, maximises the total incident energy on the *PV* modules of the *PV* plant, taking into account the shading between the rows of *PV* modules and the operating periods.
- (iii) A detailed analysis of the loads on single-axis solar tracker mounting systems, such as: weight of the structure, weight of the *PV* modules, snow loads, wind loads, and combinations thereof.
- (iv) A detailed cost analysis of single-axis solar tracker mounting systems.

The design of the row spacing and the determination of the operating periods are closely linked. Their evaluation is a key part of the calculation of the energy captured by the *PV* modules. They are therefore discussed in bullet (i).

With regard to bullet (ii), the essential part of the proposed methodology is the development of a packing algorithm that maximises the energy captured by the *PV* modules and provides answers to a number of practical questions such as: which mounting system configuration is best?, How many mounting systems can be installed?, and What is the optimal layout of the mounting systems?.

The mounting system must ensure that *PV* modules and structure remain attached during high wind speed, and that the structural capacity of the mounting system withstands the additional loads and their combinations. These verifications are carried out in bullet (iii).

The selection of a mounting system configuration for a *PV* plant with single-axis trackers is not only based on technical feasibility. The economic aspect of energy generation also plays a key role in the decision making. Therefore, the cost of the mounting system needs to be addressed comprehensively. This is discussed in bullet (iv).

The presented methodology can enable *PV* plant designers to determine the optimal distribution of single-axis solar trackers on irregular shaped parcels of land. The application of the proposed methodology results in the most efficient mounting system configuration and its optimal number, the optimal surface of the *PV* field and the maximum annual incident energy on the *PV* modules. This methodology has been applied to the Granjera photovoltaic power plant, located in Zaragoza, Spain. The mounting system configuration and its layout proposed by the methodology increases the amount of energy captured by 91.18% in relation to the current of the Granjera *PV* power plant.

The remainder of the paper is organised as follows: the background on astronomical and technical considerations, and a model to estimate the solar irradiance are shown in Section 2. The proposed methodology is explained in detail in Section 3. Section 4 presents an assessment of the economic viability. Section 5 presents the results obtained in the case of a *PV* plant located in Spain. Finally, the main conclusions of this work are drawn in Section 6.

2. Background

In order to apply the methodology presented in this paper, several previous studies have to be taken into account, such as: astronomical considerations of the Sun's motion, technical considerations of the single-axis solar tracker, periods of operation of this solar tracker (backtracking mode, limited range of motion, and normal tracking mode), and last but not least, the solar irradiance model used in the calculations.

2.1. Technical considerations of a horizontal single-axis tracking

The type of tracking system analysed in this paper has the following characteristics: horizontal single axis tracker, North–South axis alignment and East–West tracking with backtracking. This system will be called horizontal single-axis tracking. As mentioned above, this tracking system supports a number of configurations, such as 1 V, 2 V, 1H, and 2H. In practice, the most commonly used configurations are 1 V and 2 V [15]. Therefore, they are the configuration used in this study. However, the study can easily be applied to another configuration.

A horizontal single-axis tracking consists of columns, beams, spherical bearings, axis and a drive device. Fig. 1a shows a photograph of a single-axis tracker aligned with North–South axis and East–West tracking, 1 V configuration, manufactured for Gonvarri Solar Steel [15] and located at the Electrical Engineering Department of the University of Oviedo (Gijón, Spain). Fig. 1b shows a schematic of this solar tracker with 1 V configuration. The structural system has a surface treatment of Hot-Dip Galvanising. The tracking system consists of transmission system (spherical bearings), DC motor and drivers, and electronic control system. The tracking system is driven by a single engine. The *PV* modules rotate from East to West on a horizontal axis, following the Sun's daily movement. This configuration has a limited range of motion angle (β_{\max}). This range depends on the manufacturer. Typical values are $\beta_{\max} = \pm 60^\circ$ [15]. The minimum distance from the ground during operation is another consideration at the design phase.

It is common for several configurations of different sizes to be used in the same *PV* plant [15]. They have the same width, but different lengths, i.e. larger configuration and smaller configuration. For example, 1 V \times 56 (larger size) and 1 V \times 28 (smaller size).

2.2. Normal tracking mode

Normally, these solar trackers perform astronomical solar tracking that, at any given moment, seeks to minimise the angle of solar incidence [32]. Except for dual-axis tracking, it is impossible to continuously achieve the cosine of the angle of incidence to unity. In the case of the horizontal single-axis tracking, the minimisation is achieved by matching tracker rotation to the projection of the Sun's position onto the tracking plane of rotation. It is a solar tracker that at noon passes over its horizontal surface, but with continuous movement during the day to follow the solar altitude α_s .

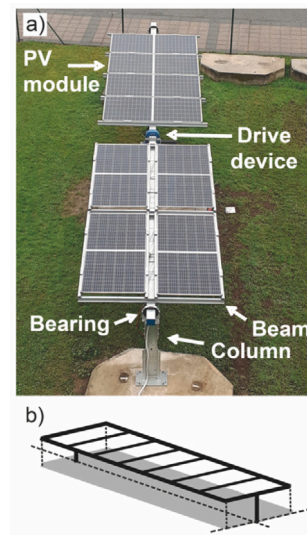


Fig. 1. Representation of a horizontal single-axis tracking.

2.3. Backtracking mode

During low solar elevation intervals (sunrise and sunset) the highest incidence of self-shading occurs between the *PV* modules. To avoid this phenomenon, a technique known as backtracking is used [33]. This technique consists of varying the tilt angle (β_B) of the *PV* modules so that the shadows of each row of *PV* modules are not projected onto the row behind. Although, this solar tracking does not achieve maximum solar irradiance capture, the negative effect of this reduction is compensated by the absence of hot spots [34].

2.4. Determination of solar irradiance in the plane of array

The total solar irradiance incident on a tilted plane consists of three components [32]: beam component, diffuse component and ground-reflected component. The determination of the beam component is straightforward [32]. The determination of the other two components is more complex and admits several interpretations.

Casares de la Torre et al. [33] presented a study analysing the conversion of *PV* installations with horizontal single-axis tracking configuration into agrivoltaic installations. To determine the diffuse irradiance incident on the *PV* modules, three models were considered: Liu–Jordan isotropic model [35], Hay–Davies anisotropic model [36], and Perez's anisotropic model [37]. The results showed great similarity with the three models. In another study, Mehleri et al. [38] compared 4 isotropic and 7 anisotropic models. They conclude that the most accurate results were produced with the Liu and Jordan model [35]. The isotropic model proposed by Liu and Jordan [35] assumes that the diffuse irradiance is uniform over the sky. This model has been validated in different places and is recognised worldwide [39–41]. Therefore, it can be assumed that the use of this simplified model allows valid results to be extracted. This model has been used in this work.

The irradiance reflected from the ground is essentially impossible to compute it precisely, due to the many factors contributing to it [32]. Therefore, the irradiance reflected from the ground is also considered isotropic [35]. This assumption and the equation proposed by Liu and Journal [35] for its determination is assumed by most authors [36,37,39–41].

To calculate the total solar irradiance incident on a tilted plane, it is necessary to previously know the beam and diffuse horizontal irradiances [32]. It is well known that the distribution of annual solar irradiance is site-specific and shows considerable variations due to the

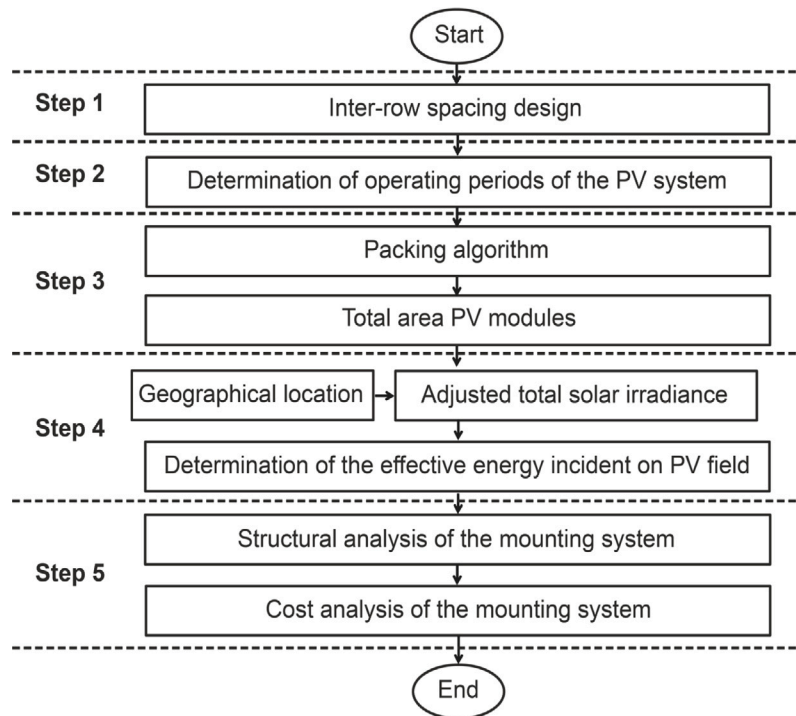


Fig. 2. A flowchart outlining the proposed methodology.

distribution of local cloud cover [42]. In the absence of meteorological data from ground-level meteorological stations, these solar irradiances can be estimated by different models such as clear-sky models [40], satellite-based models [43], temperature-based methods [44], etc. For this purpose, the model proposed by [45] is used in this paper. This method determines the adjusted hourly solar irradiance on horizontal surfaces, both beam and diffuse. The term “adjusted” indicates that the weather conditions at each location are considered. This model has been validated in different places [45]. As this method incorporates the meteorological conditions of each location, it gives good results and has been used in several studies [11,21,46]. The adjusted hourly beam and diffuse solar irradiance on a horizontal surface to the weather conditions of a particular site calculated following the method proposed by [45] are denoted as \mathbb{I}_{bh} and \mathbb{I}_{dh} , respectively.

The total solar irradiance incident on a tilted plane can be expressed as follows [32]:

$$\mathbb{I}_t(n, \beta, T) = \mathbb{I}_{bh}(n, T) \cdot \frac{\cos \theta_i}{\cos \theta_z} + \mathbb{I}_{dh}(n, T) \cdot \left(\frac{1 + \cos \beta}{2} \right) + (\mathbb{I}_{bh}(n, T) + \mathbb{I}_{dh}(n, T)) \cdot \rho_g \cdot \left(\frac{1 - \cos \beta}{2} \right) \quad (1)$$

where $\mathbb{I}_{bh}(n, T)$ (W/m^2) is the adjusted beam solar irradiance on a horizontal surface, $\mathbb{I}_{dh}(n, T)$ (W/m^2) is the adjusted diffuse solar irradiance on a horizontal surface, n (day) is the day of the year, β ($^\circ$) is the tilt angle, θ_z ($^\circ$) is the zenith angle of the Sun, ρ_g is the ground reflectance (dimensionless), T (h) is the solar time, and θ_i ($^\circ$) is the incident angle.

The ground reflectance varies with the type and rugosity of the land, the spacing between rows of PV modules, shadows from other PV modules, or position of the Sun [34]. Due to the difficulty of correctly estimating the instantaneous ground reflectance, it has been assumed a constant value.

On the other hand, the incident angle θ_i can be calculated for each operating period of the solar tracker as [32]:

- In normal tracking mode, β , with the well-known equation:

$$\cos \theta_i = \sqrt{\cos^2 \theta_z + \cos^2 \delta \sin^2 \omega} \quad (2)$$

In limited range of motion, β_{max} :

$$\cos \theta_i = \cos \beta_{max} \cos \theta_z + \sin \beta_{max} \sin \theta_z \cos (\gamma_S - \gamma) \quad (3)$$

In backtracking mode, β_B :

$$\cos \theta_i = \cos \beta_B \cos \theta_z + \sin \beta_B \sin \theta_z \cos (\gamma_S - \gamma) \quad (4)$$

where β ($^\circ$) is the tilt angle, β_{max} ($^\circ$) is the limited range of motion, β_B ($^\circ$) is the backtracking angle, θ_z ($^\circ$) is the zenith angle of the Sun, γ ($^\circ$) is the azimuth angle, γ_S ($^\circ$) is the azimuth of the Sun, δ ($^\circ$) is the solar declination, and ω ($^\circ$) is the hour angle.

3. Methodology

The optimal design of a PV plant can be formulated as an objective function with a set of constraints. The problem variables are very high as discussed above. The objective function can be defined on the basis of energy or economic criteria, and the constraints are usually of a technical nature. Therefore, due to the large number of variables, this work has been limited to optimising the following aspects of PV plant design: (i) maximising the amount of solar irradiance falling on the PV modules, (ii) avoiding the phenomenon of self-shading between PV modules, and (iii) minimising the levelised cost of electricity (LCOE). In order to achieve the proposed goals, a methodology was developed. This consists of the following steps: (i) Inter-row spacing design; (ii) Determination of operating periods of the PV system; (iii) Optimal number of solar trackers; and (iv) Determination of the effective annual incident energy on photovoltaic modules. A flowchart outlining the proposed methodology is shown in Fig. 2.

A PV plant with horizontal single-axis tracking is considered. Fig. 3 shows a schematic of a PV plant with this tracking system and 1 V configuration. As shown in Fig. 3, each mounting system can be characterised by several parameters: length of the mounting system (L), width of the mounting system (W), height of the column (p), and minimum distance on the ground (e_s). The distance $E-W$ from column to column of two adjacent mounting systems is the pitch (e_t). The $N-S$ distance between adjacent mounting systems is the longitudinal distance (e_l). It is necessary to leave a distance $E-W$ (d_{min}) between two adjacent

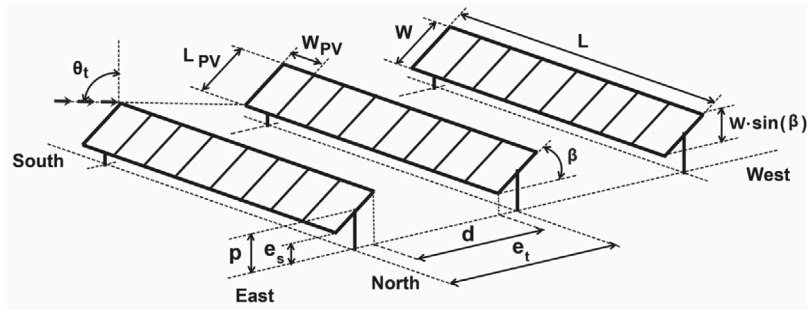


Fig. 3. Representation of a horizontal single-axis tracking.

mounting systems for cleaning and maintenance. In addition, each PV module can also be characterised by: length of a PV module (L_{PV}), and width of a PV module (W_{PV}).

The transverse angle θ_t ($^\circ$) is given by [32]:

$$\theta_t = \arctan(\tan \theta_z |\sin \gamma_s|) \tag{5}$$

In normal tracking mode, the tracking angle β ($^\circ$) is the solar transversal angle θ_t ($^\circ$) [32]:

$$\beta = \theta_t \tag{6}$$

In order to achieve the stated goals, the following conditions are assumed:

- (i) The land can be of any irregular shape and is flat. Land selection and geographical location are not the focus of this study.
- (ii) Horizontal single-axis tracking will be used in this study.
- (iii) Although, the number of commercial PV module models is very high, only one model is considered in this study. The use of another PV module model would only affect the dimensions of the mounting system, so the procedure would be the same.
- (iv) The choice of mounting system configuration is limited to the models most commonly used in PV plants [15], the 1 V and 2 V. However, the proposed algorithm could use another type of mounting system configuration.
- (v) From a practical point of view, it is necessary to consider a longitudinal distance (e_t) to facilitate the passage between the mounting systems [15].
- (vi) A minimum transverse maintenance distance (d_{min}) between rows of mounting systems is considered to allow for proper inspection, cleaning and maintenance. This value shall be taken with the solar tracker in its limited range of motion angle, β_{max} .
- (vii) The solar tracker has a limited range of motion. This range depends on the manufacturer. Typical values are $\beta_{max} = \pm 60$ ($^\circ$) [15].
- (viii) A minimum distance on the ground (e_s) of the mounting systems is considered. A typical value is $e_s = 0.4$ (m) [15].

3.1. Inter-row spacing design

During the initial design phase of a PV plant there are several parameters that can be easily modified and that affect the profitability of the project. One of these parameters is the inter-row spacing. The amount of shade depends on this parameter, therefore this parameter plays a very important role. Therefore, this methodology starts with the inter-row spacing design. In normal tracking mode, one row of solar PV modules can cause a shadow on the other row if the adequate inter-row spacing is not taken into account when designing the PV plant. Inter-row shading causes lower energy production and can also damage PV modules by developing hot spots. Eliminating the impact of shading can be achieved by increasing the inter-row spacing, but this decision increases the initial investment costs (land costs, and wiring costs).

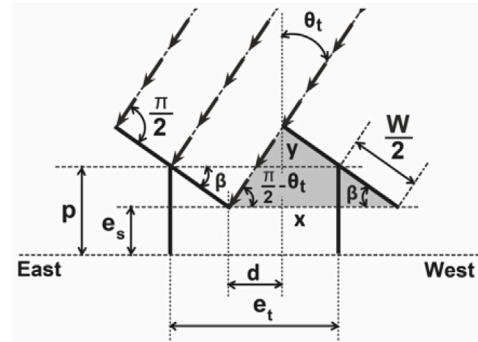


Fig. 4. Detail of the transversal study of the installation.

Two approaches can be applied in inter-row spacing design: one is based on a minimum required distance between the rows for the maintenance of the solar field, and the other is based on avoiding mutual shading between the rows of PV modules. These two approaches have to be fulfilled at the same time.

In this paper, mathematical equations will be proposed to determine the inter-row spacing of PV modules. To take into account the self-shading between the rows of PV modules, the parameters shown in Fig. 4 are used. Three of these parameters are subject to restrictions that have to be fulfilled simultaneously: β_{max} , d_{min} and θ_t .

The restrictions to be taken into account are:

- (i) The solar tracker has a limited range of motion β_{max} and a minimum distance on the ground (e_s). These parameters are used to obtain the minimum column height, p (m).
- (ii) It is necessary to consider a minimum distance between rows of trackers, d_{min} , to allow a proper inspection, cleaning, and maintenance.
- (iii) Inter-row spacing should be estimated for minimum shading losses. To minimise the effects of inter-row shading various technical reports have been published by different governments. For example, the Institute for Energy Diversification and Saving of the Spanish Government [31] states that the distance between PV modules has to guarantee a minimum of 4 hours of sunshine around noon on the Winter solstice. For this purpose, the solar transversal incidence angle given by 21 December at 10 : 00 is denoted by θ_{tst} . The θ_{tst} depends strongly on the location's latitude and it can be calculated using Eq. (5) and the solar angles, θ_z and γ_s , for 21 December at 10 : 00:

$$\theta_{tst} = \arctan(\tan \theta_z |\sin \gamma_s|) \tag{7}$$

From Fig. 4 it can be immediately deduced that the minimum height of the column is given by:

$$p = \frac{W}{2} \sin \beta_{max} + e_s \tag{8}$$

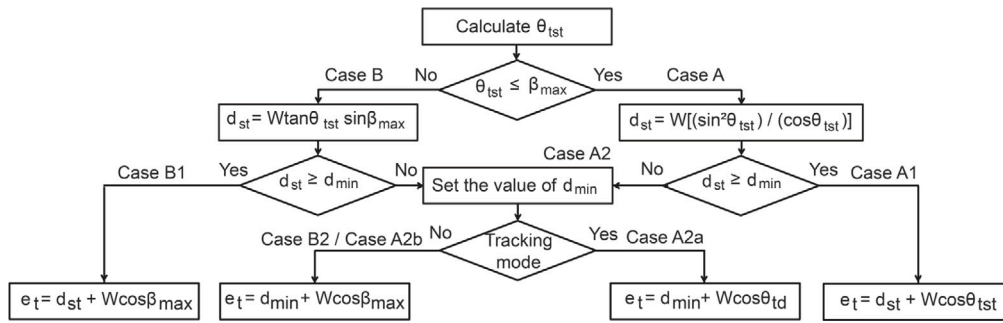


Fig. 5. A flowchart outlining the proposed inter-row spacing design.

The parameter d follows immediately from Fig. 4 that for any value of β and θ_t is true:

$$d = W \tan \theta_t \sin \beta \tag{9}$$

And therefore, the parameter e_t can be expressed as:

$$e_t = d + W \cos \beta \tag{10}$$

Since in normal tracking mode, Eq. (6) is satisfied, the parameters d and e_t can be expressed as:

$$d = W \frac{\sin^2 \theta_t}{\cos \theta_t} \tag{11}$$

$$e_t = \frac{W}{\cos \theta_t} \tag{12}$$

To calculate the pitch e_t , we will consider simultaneously the three restrictions mentioned above: β_{\max} , d_{\min} , and θ_{tst} . A flowchart outlining the proposed procedure is shown in Fig. 5.

To obtain e_t , the next steps are to be followed:

- (A) Once θ_{tst} has been calculated and $\theta_{tst} \leq \beta_{\max}$, this value is reached at normal tracking mode ($\beta = \theta_t$), and therefore from (11) we have that the distance d in this case is:

$$d_{st} = W \frac{\sin^2 \theta_{tst}}{\cos \theta_{tst}} \tag{13}$$

But there are two possible cases: A1 and A2.

- (A1) If $d_{st} \geq d_{\min}$ then, with this design we are guaranteed to meet all three restrictions. Therefore,

$$e_t = d_{st} + W \cos \theta_{tst} \tag{14}$$

- (A2) If $d_{st} < d_{\min}$ then, we must take the value of d_{\min} . In case A2 there are two possible cases: A2a and A2b. It is fulfilled:

(A2a) If $\theta_{st} < \theta_{tst}$ then,

$$e_t = d_{\min} + W \cos \theta_{td} \tag{15}$$

(A2b) If $\theta_{st} > \theta_{tst}$ then,

$$e_t = d_{\min} + W \cos \beta_{\max} \tag{16}$$

- (B) If $\theta_{tst} > \beta_{\max}$ then that position cannot be reached by the tracker. The tracker will be at position $\beta = \beta_{\max}$ and Eq. (9) will be used:

$$d_{st} = W \tan \theta_{tst} \sin \beta_{\max} \tag{17}$$

But there are two possible cases: B1 and B2.

- (B1) If $d_{st} \geq d_{\min}$ then, with this design we are guaranteed to meet all three restrictions. Therefore,

$$e_t = d_{st} + W \cos \beta_{\max} \tag{18}$$

- (B2) Si $d_{st} < d_{\min}$ then, we must take the value of d_{\min} . Therefore,

$$e_t = d_{\min} + W \cos \beta_{\max} \tag{19}$$

Table 1

Operating periods of the solar tracker for the most general case.

Operating period	Start	End	Tilt angle
Backtracking mode	T_R	T_{b1}	$\beta = \beta_B$
Limited range of motion	$T_{\beta1}$	$T_{\beta2}$	$\beta = -\beta_{\max}$
Normal tracking mode	$T_{\beta1}$	$T_{\beta2}$	$\beta = \theta_t$
Limited range of motion	$T_{\beta2}$	T_{b2}	$\beta = \beta_{\max}$
Backtracking mode	T_{b2}	T_S	$\beta = \beta_B$

3.2. Determination of operating periods of the PV system

The determination of the operating periods of the horizontal single-axis tracking is essential to determine the annual effective energy incident on PV modules and for the design of the solar tracking system.

Figs. 6 and 7 show the operating periods of the solar tracker in cases A and B, respectively. In these figures, two or three zones of operation can be distinguished: (i) Backtracking mode; (ii) Limited range of motion, and (iii) Normal tracking mode.

In Figs. 6 and 7, $T_R(n)$ (hour) is the sunrise solar time, $T_{b1}(n)$ (hour) is the end of the backtracking mode, $T_{\beta1}(n)$ (hour) is the start of the normal tracking mode, $T_{\beta2}(n)$ (hour) is the end of the normal tracking mode, $T_{b2}(n)$ (hour) is the start of the backtracking mode, and $T_S(n)$ (hour) is the sunset solar time.

Table 1 summarises the different operating periods of the solar tracker for the most general case. where β_B (°) is the backtracking angle, and β_{\max} (°) is the limited range of motion angle.

The sunrise solar time $T_R(n)$ and sunset solar time $T_S(n)$ can be determined by classical equations [32]. When $\beta = \mp\beta_{\max}$ in Eq. (5) the interval $[T_{\beta1}(n), T_{\beta2}(n)]$ can be determined. The determination of $T_{b1}(n)$ and $T_{b2}(n)$ is more complex. A flowchart outlining with the proposed procedure for the determination of these parameters is shown in Fig. 8.

To obtain $T_{b1}(n)$ and $T_{b2}(n)$, it is necessary to take into account:

- (i) This section uses the same cases studied in the inter-row spacing design section. The variable θ_{td} is obtained from the corresponding equation and $\theta_{tb} = \theta_{td}$.

- (ii) Case A2 can be divided into two scenarios, A2a and A2b:

In case A2a, it is assumed that we are in normal tracking mode and of the equation:

$$d_{\min} = W \frac{\sin^2 \theta_{td}}{\cos \theta_{td}} \tag{20}$$

The variable θ_{td} is obtained. If $\theta_{td} < \beta_{\max}$ is satisfied, the above calculation is correct, and $\theta_{tb} = \theta_{td}$. If $\theta_{td} > \beta_{\max}$ is satisfied, the above calculation is NOT correct and case A2b must be considered. In A2b case, the following equation should be used:

$$d_{\min} = W \tan \theta_{td} \sin \beta_{\max} \tag{21}$$

The variable θ_{td} is obtained and $\theta_{tb} = \theta_{td}$.

Once θ_{tb} is determined, using Eq. (5), $T_{b1}(n)$ and $T_{b2}(n)$ can be determined.

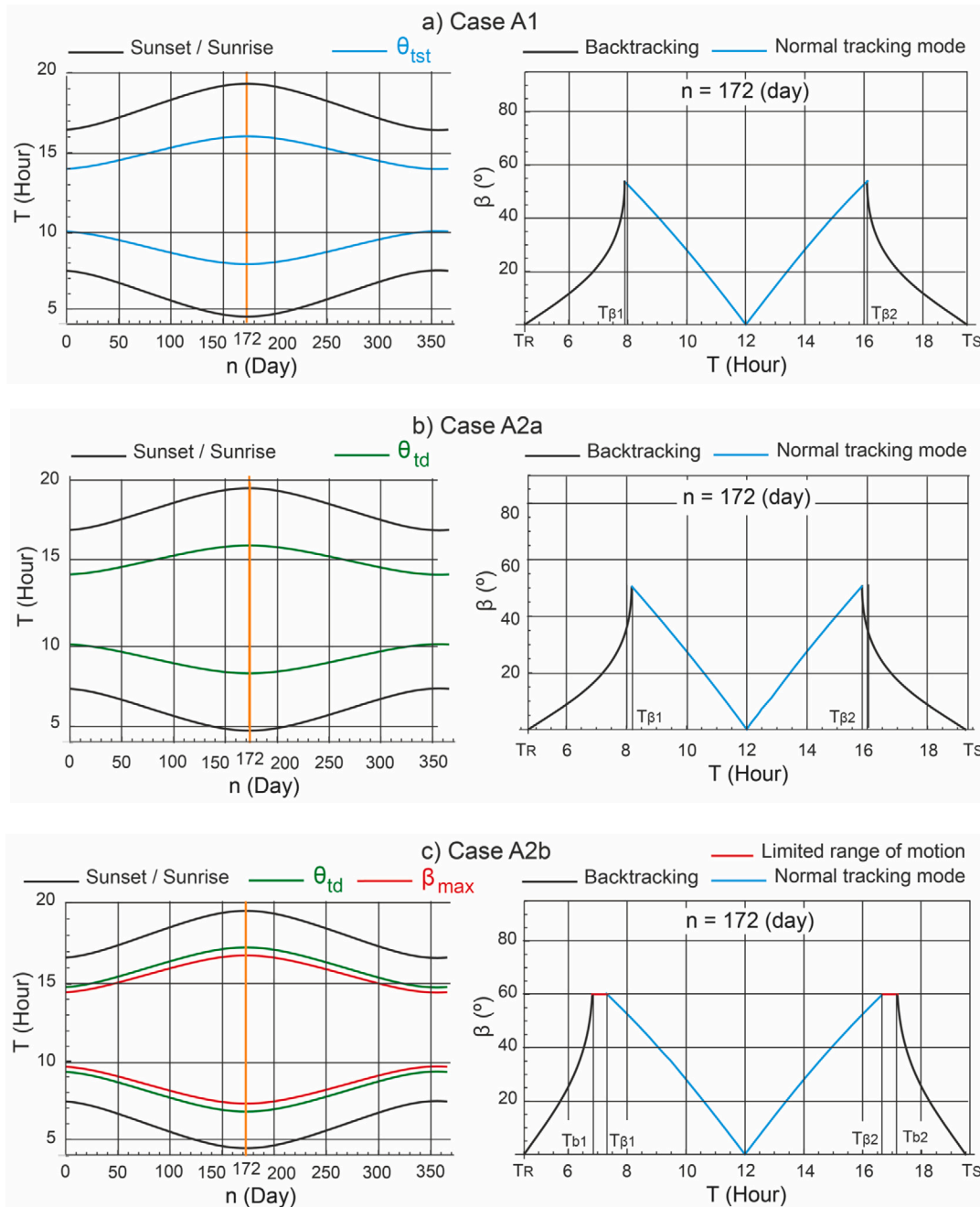


Fig. 6. Operating periods of the solar tracker: Case A.

In some cases, depending on the value of the limited range of motion or the configuration under study, the operating periods are only two: backtracking mode and normal tracking mode. That is, from the operating period of backtracking mode, it goes directly to the normal tracking mode.

Below are some examples, which show the importance of the use of the possible operating cases of the solar tracker:

- (i) Case A1 is presented in Fig. 6a. It represents a PV plant with horizontal single-axis tracking, 2 V configuration, located in Barcelona (Spain) with latitude $41^{\circ}23'19''N$, longitude $2^{\circ}9'32''E$ and altitude 13 (m). In this case: $\theta_{tst} = 53.98 (^{\circ}) < \beta_{max} = 60 (^{\circ})$, $d_{st} = 4.72 (m) > d_{min} = 4 (m)$.
- (ii) Case A2a is presented in Fig. 6b. It represents a PV plant with horizontal single-axis tracking, 2 V configuration, located in Almeria

(Spain) with latitude $36^{\circ}50'07''N$, longitude $2^{\circ}24'08''W$ and altitude 22 (m). In this case: $\theta_{tst} = 49.04 (^{\circ}) < \beta_{max} = 60 (^{\circ})$, $d_{st} = 3.69 (m) < d_{min} = 4 (m)$, $\theta_{td} = 50.63 (^{\circ})$.

- (iii) Case A2b is presented in Fig. 6c. It represents a PV plant with horizontal single-axis tracking, 1 V configuration, located in Barcelona (Spain) with latitude $41^{\circ}23'19''N$, longitude $2^{\circ}9'32''E$ and altitude 13 (m). In this case: $\theta_{tst} = 53.98 (^{\circ}) < \beta_{max} = 60 (^{\circ})$, $d_{st} = 2.34 (m) < d_{min} = 4 (m)$, $\theta_{td} = 65.44 (^{\circ})$.
- (iv) Case B1 is presented in Fig. 7a. It represents a PV plant with horizontal single-axis tracking, 2 V configuration, located in Berlin (Germany) with latitude $52^{\circ}31'12''N$, longitude $13^{\circ}24'36''E$ and altitude 34 (m). In this case: $\theta_{tst} = 69.87 (^{\circ}) > \beta_{max} = 60 (^{\circ})$, $d_{st} = 10.03 (m) > d_{min} = 4 (m)$.
- (v) Case B2 is presented in Fig. 7b. It represents a PV plant with horizontal single-axis tracking, 1 V configuration, located in Paris

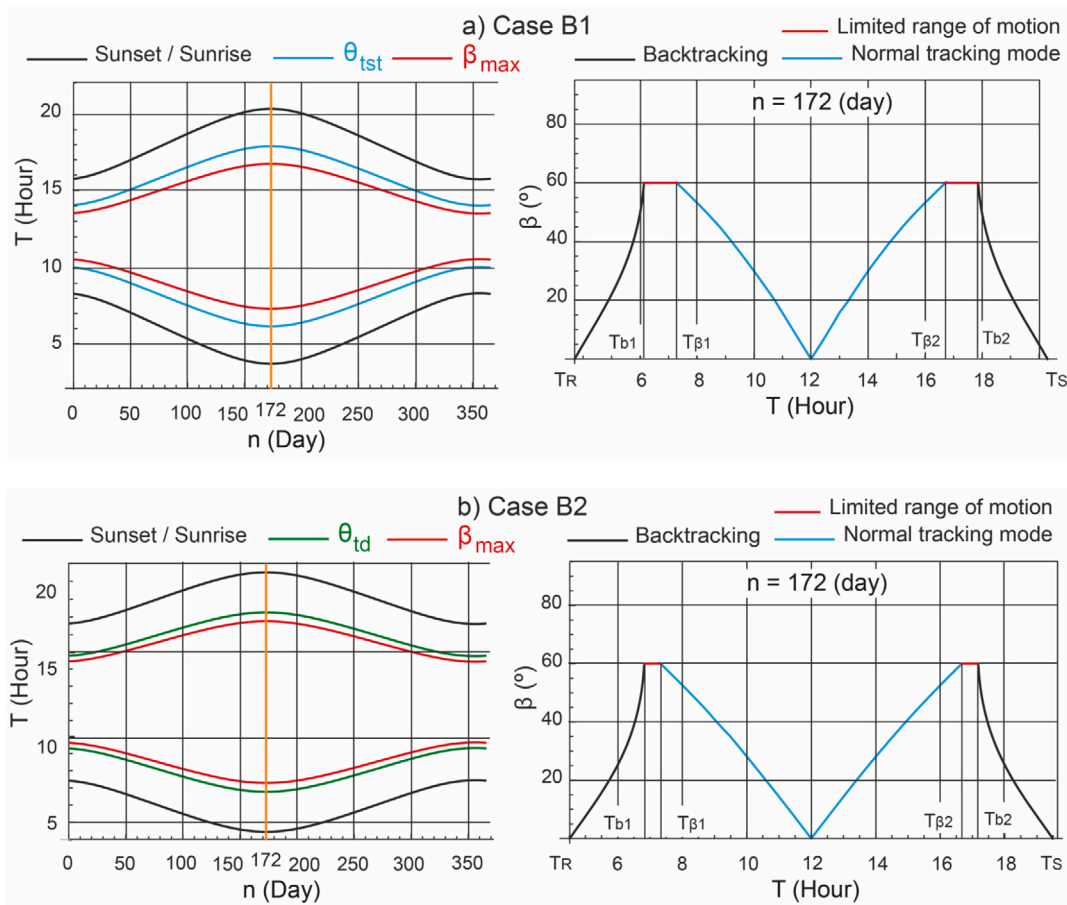


Fig. 7. Operating periods of the solar tracker: Case B.

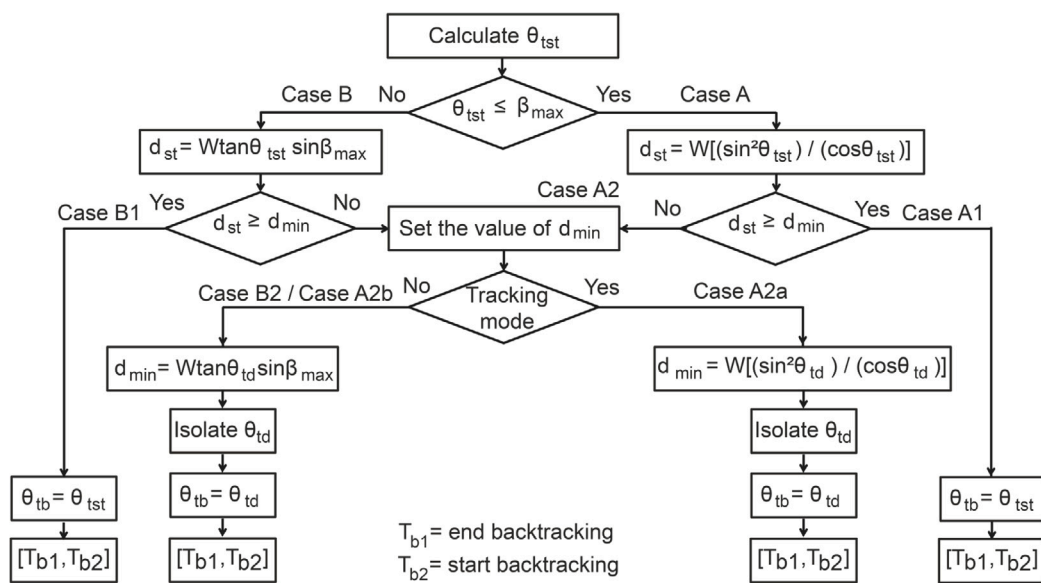


Fig. 8. A flowchart outlining the determination of operating periods of the PV system.

(France) with latitude $48^{\circ}51'12''N$, longitude $2^{\circ}20'55''E$ and altitude 35 (m). In this case: $\theta_{st} = 64.01$ ($^{\circ}$) $> \beta_{max} = 60$ ($^{\circ}$), $d_{st} = 3.74$ (m) $< d_{min} = 4$ (m), $\theta_{td} = 65.44$ ($^{\circ}$).

3.3. Backtracking algorithm

The backward strategy eliminates shadows between the PV modules during low solar elevation intervals (sunrise and sunset). When no slope in the land is considered, a standard backtracking sets all rows to the same angle.

From Eq. (10) the backtracking algorithm can be derived:

$$e_t = W \left(\frac{\sin \beta}{\cot \theta_t} + \cos \beta \right) \tag{22}$$

By performing the following mathematical operations:

$$\frac{e_t}{W} = \frac{\sin \beta}{\cos \theta_t} \sin \theta_t + \cos \beta \tag{23}$$

$$\frac{e_t}{W} \cos \theta_t = \sin \beta \sin \theta_t + \cos \beta \cos \theta_t = \cos(\theta_t - \beta) \tag{24}$$

$$\theta_t - \beta = \arccos \left(\frac{e_t}{W} \cos \theta_t \right) \tag{25}$$

the backtracking angle, β_B is calculated according to the following equation:

$$\beta_B = \theta_t - \arccos \left(\frac{e_t}{W} \cos \theta_t \right) \tag{26}$$

In the previous section, the solar transverse angle was calculated to mark the principle of backtracking, θ_{tb} .

The derived Eq. (26) is similar to that presented by other authors, such as [47].

3.4. Optimal number of solar trackers

In the design of a PV plant with solar tracking, it is not only the solar tracking strategies implemented that determine the energy produced.

A specific packing algorithm implemented in the *Mathematica*[™] software has been designed for this problem. The algorithm shares certain ideas with the one presented in [11], although they are different nature. In the work presented by [11], fixed tilt angle mounting systems were optimally packaged by calculating their optimum tilt angle, whereas the present work deals with single-axis trackers. In this case the problem consists in the maximisation of total PV modules area, choosing the position of the solar trackers on a large area of land. For this purpose, the projection on the horizontal plane of the solar trackers in their noon position ($\beta = 0$ ($^{\circ}$)) is considered.

For the development of the packing algorithm, input variables and variables determined in the previous sections have to be taken into account: (i) Length of the mounting system, L (m); (ii) Longitudinal distance between solar trackers, e_t (m); and (iii) Pitch, e_r (m). All other variables have already been taken into account in the inter-row spacing design, such as β_{max} , d_{min} , and θ_{st} .

Like other similar studies [11], this work uses GIS (Geographic Information System) techniques to determine the UTM (Universal Transverse Mercator) coordinates of the available land area. Specifically, the software used is the QGIS[™], because it is free software with an open code [48,49].

Normally two sizes of mounting systems are used in the same PV plant [15]. They have the same width, but different lengths, i.e. larger size and smaller size. Therefore, the packing algorithm is designed to optimally combine these two sizes. In this work, the 1 V \times 56, or 2 V \times 56, (larger size) and 1 V \times 28, or 2 V \times 28, (smaller size) configurations have been considered. However, the packing algorithm allows other configurations to be used. Although the PV plant is composed of a higher number of larger configurations due to economic considerations, it is common to use the smaller configurations to make better use of the irregularities in the contour of the available land area.

The objective function is maximising the total PV modules area (A_{TPV}):

$$A_{TPV} = \sum_{i=1}^{N_{PV}} W_{PV} \cdot L_{PV} \tag{27}$$

where N_{PV} is the number of PV modules, W_{PV} (m) is the width of a PV module, and L_{PV} (m) is the length of a PV module. The objective function is subject to two constraints, such as: the pitch e_r , and the longitudinal distance between solar trackers e_t .

Fig. 9. shows the schematic of a PV plant with $N - S$ orientation single-axis tracking. The PV modules are represented by rectangles inside the mounting system. The packing scheme consists of placing rows of solar trackers to the North–South direction, with dimensions $W \times L$ inside the available land area \bar{P} (see Fig. 9.a). Although W is not a decision variable in the packing algorithm, as it is included in the pitch e_r , Fig. 9.b shows a value of W which is the projection caused at noon ($\beta = 0$ ($^{\circ}$)) by each mounting system. It is evident that this value is time-varying, between $[-\beta_{max}, \beta_{max}]$ with $S = W \cos \beta$.

For the explanation of the method, the projection on the horizontal plane of each mounting system has to be considered. The shape of this projection is a rectangle of dimensions $W \times L$ (see Fig. 9.b). All these rectangles R_{ij} have the axis of rotation oriented to North–South. The method gets the dimensions of the land area \bar{P} , and consider the minimum rectangle R , where \bar{P} is inscribed. The sides of R , are the reference axes ($x - y$) with the $N - S$ direction as the positive axis y , and the lower left corner of the rectangle R , is taken as the origin O .

The base rectangle R_{11} is defined using the vertex A on the origin O of the rectangle R :

$$R_{11} = \{A(0, 0), B(W, 0), C(W, L), D(0, L)\} \tag{28}$$

Taking:

$$\Delta x = e_t; \quad \Delta y = L + e_l \tag{29}$$

the packing pattern adds rectangles R_{ij} defined as:

$$R_{ij} = \{A((j - 1)\Delta x, (i - 1)\Delta y), B((j - 1)\Delta x + W, (i - 1)\Delta y), C((j - 1)\Delta x + W, (i - 1)\Delta y + S), D((j - 1)\Delta x, (i - 1)\Delta y + S)\} \tag{30}$$

In other studies in the literature, packing algorithms were used with mounting systems without solar tracking (e.g. [11]) considering the tilt angle was a decision variable, as was the type of commercial PV module and the mounting system configuration. With these characteristics, the computation time of the algorithm increased significantly, as there were many possible combinations to be considered by the full exploration of the search space. However, in this work, only 2 mounting system configurations are previously chosen by the designer.

Once the variables L , e_r , and e_l have been chosen, the only variable to consider will be the discretisation that will be introduced to remove the restriction on the fact that the vertex A of the basis rectangle R_{11} is O . This allows multiple packings to be considered and the one that best suits the irregularities of the contour of the available land area P to be chosen. To get this, the algorithm chooses different points for the vertex A of R_{11} inside the area $\Delta x \times \Delta y$ highlighted in Fig. 9.c. Given the dimensions of the mounting system it is interesting to consider 2 types of discretisations: m_x and m_y . Outside this area $\Delta x \times \Delta y$ this arrangement repeats again.

Once the $m_x \times m_y$ possible combinations have been analysed, the algorithm provides the best arrangement of the mounting systems, this is, the maximum of A_{TPV} . The algorithm fills first with the larger configuration and then with the smaller configuration completes the irregularities of the available land area. More details will be provided in the results section.

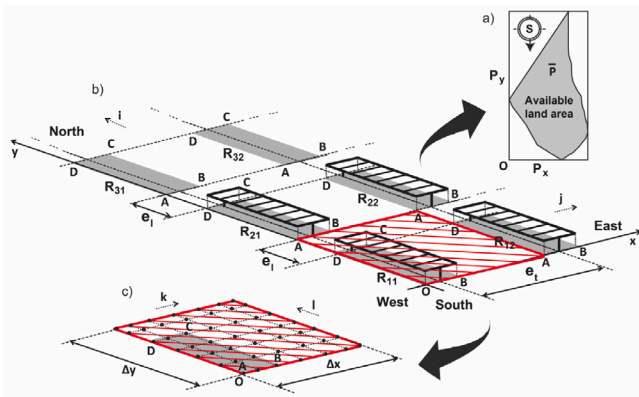


Fig. 9. Packing algorithm.

3.5. Effective annual energy incident on PV modules

In the design of PV plants composed of mounting systems without a solar tracker (e.g. [11]), it is essential to study the shadows produced between the rows of mounting systems. In contrast, in this study, when considering solar tracking mounting systems with backtracking movement, the shading phenomenon will never occur.

As the shading effect does not occur, the total area A_{TPV} is constant and, the total energy $E_{TPV}(n)$ for each day of the year, n , can be determined by calculating the adjusted irradiance, $\mathbb{H}_i(n)$ and multiplying by the total area A_{TPV} obtained from the packing algorithm:

$$E_{TPV}(n) = \mathbb{H}_i(n) \cdot A_{TPV} \quad (31)$$

For the calculation of $\mathbb{H}_i(n)$, according to Fig. 8, it must be taken into account that each day n of the year has certain operating periods in which the tilt angle β varies. Without loss of generality, Eq. (32) represents the case that will be studied in the results section. The 5 zones into which the operation period is decomposed are:

$$\begin{aligned} \mathbb{H}_i(n) = & \int_{T_{R(n)}}^{T_{B1(n)}} \mathbb{H}_i(n, \beta_B, T) dT + \int_{T_{B1(n)}}^{T_{\beta1(n)}} \mathbb{H}_i(n, -\beta_{max}, T) dT + \\ & + \int_{T_{\beta1(n)}}^{T_{\beta2(n)}} \mathbb{H}_i(n, \theta_i, T) dT + \int_{T_{\beta2(n)}}^{T_{B2(n)}} \mathbb{H}_i(n, \beta_{max}, T) dT + \int_{T_{B2(n)}}^{T_{S(n)}} \mathbb{H}_i(n, \beta_B, T) dT \end{aligned} \quad (32)$$

4. Assessment of the economic viability

Two alternative mounting system configurations, 1 V and 2 V, are considered in this study. The assessment of the economic viability of each configuration studied is a key element in making an investment decision. Therefore, the objective of this section is to measure the economic value of each of the two configurations.

The assessment of the economic viability is formulated using the initial investment costs, operation and maintenance costs, as well as the total energy generation, during the lifetime period of the PV modules. For this purpose, the levelized cost of the produced electrical energy (LCOE) is determined. The LCOE is defined by Branker et al. [50] as the ratio between the life-cycle cost of the PV system and the whole life produced energy. The LCOE in (€/kWh) of a PV system is expressed in the following equation [50]:

$$LCOE = \frac{\sum_{i=0}^I [C_{Ti} / (1+r)^i]}{\sum_{i=0}^I [S_i / (1+r)^i]} \quad (33)$$

where C_{Ti} is the total cost of the project for i (€), S_i is the total electrical energy output for i (kWh), I is the lifetime of the project (years), r is the discount rate for i , and i is the year.

4.1. Total cost of a large-scale PV plant

The total cost of a large-scale PV plant during its lifetime depends not only on the initial investment cost, but also on the operation and maintenance costs. The first can be determined with some ease, while the second are more difficult to determine.

As there is no standardisation for Operation and Maintenance costs [51], it is difficult to determine them. Mortensen [52] suggests that these costs with solar tracking systems are twice as high as those without solar tracking. The National Renewable Energy Laboratory recommends assuming an annual operation and maintenance costs of 0.5% of the initial investment cost for large systems [53]. This recommendation has been taken into account in this study.

The initial investment cost components are as follows: total number of PV modules (N_{PV}), unit cost of a PV module (C_{PV}) in (€/unit), total number of mounting systems (N_{MS}), unit cost of the mounting systems (C_{MS}) in (€/unit), total number of electric motors (N_{EM}), unit cost of the electric motor (C_{EM}) in (€/unit), total number of control systems (N_{CS}), unit cost of the control system (C_{CS}) in (€/unit), total number of inverters (N_{inv}), unit cost of the inverter (C_{inv}) in (€/unit), cost of the land area (C_L) in (€), cost of the cable (C_{Cb}) in (€), cost of the transformer (C_T) in (€), cost of the protection devices (C_{PD}) in (€), and cost of the monitoring system (C_M) in (€). Obviously, these costs are highly dependent on site-specific parameters.

In this paper, the available land area is considered to be a constant parameter, so the following components of the initial investment cost can also be considered to be constant: C_L , C_{Cb} , C_T , C_{PD} , and N_{inv} . Although, the C_{inv} could slightly vary with each configuration, its value has also been considered to be constant. The remaining parameters will depend on the configuration analysed. The values N_{PV} , N_{MS} , N_{EM} , and N_{CS} are output parameters of the proposed algorithm. C_{PV} , C_{EM} , and C_{CS} are given by the manufacturers. Finally, a structural analysis is necessary to determine C_{MS} , as the weight of the mounting system defines its cost. According to these conditions, the initial investment cost can be determined as follows:

$$C_i = N_{PV} \cdot C_{PV} + N_{MS} \cdot C_{MS} + N_{EM} \cdot C_{EM} + N_{CS} \cdot C_{CS} + K \quad (34)$$

4.2. Costs analysis of the mounting system

According to literature, the initial investment costs of the mounting systems represent a significant part of the total cost of a large-scale PV plant [54]. Due to the rising cost of raw materials [55] and the falling cost of PV modules [10], this influence is increasing.

The weight of the different elements of the mounting system determines the cost of the structure, C_{MS} . For this it is necessary to determine the profiles to be used for its manufacture, and therefore a structural study is essential. The results are shown in Annex D.

4.2.1. Structural analysis of the mounting system

The cost of the mounting system is directly related to the loads that you have to bear, such as wind loads, snow loads, etc. Therefore, this section explains in detail the calculation of the loads affecting the mounting system.

The mounting system must be able to withstand during its lifetime: (i) its weight; (ii) the weight of the PV modules; (iii) the wind load; (iv) the weight of accumulated snow; and (v) the combination of the above loads. Although, wind action plays a major role in the design of the mounting system, other loads must also be considered, especially in the combination of loads. The procedure used in [11] is applied in the present study. The results are shown in Annexes A and B. The cost of the mounting system is directly related to the accurate estimation of the magnitudes of these loads.

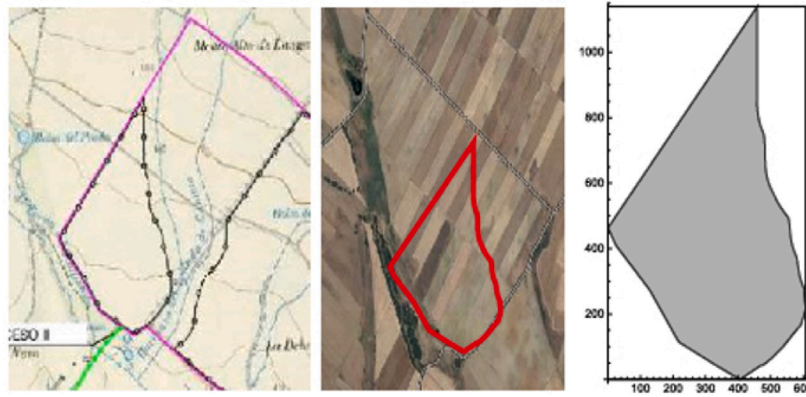


Fig. 10. Location of the Granjera PV power plant and parcel \bar{P} .

4.3. Total electrical energy output

In this study, two different configurations are studied. Therefore, the energy generated by the PV plant is calculated according to the selected configuration. In both configurations, the total electrical energy output of the PV plant is calculated in accordance with the following equation:

$$S_i = E_i \cdot \eta \cdot (1 - d_r)^i \tag{35}$$

where S_i is the total electrical energy output at the i th year (kWh), E_i is the availability of solar resource at the i th year (kWh), η is the performance factor, d_r is the annual degradation rate, and i is the year.

4.4. LCOE Efficiency

Following the definition of absolute LCOE, several authors introduce the term “LCOE efficiency” [2,56]. This parameter facilitates comparison of different mounting systems, solar tracking systems, module PV technologies, etc. The LCOE efficiency can be defined as the ratio of the LCOE of the 1 V configuration ($LCOE_{1V}$) and the LCOE of the 2 V configuration ($LCOE_{2V}$):

$$\eta_{LCOE} = \frac{LCOE_{1V}}{LCOE_{2V}} \tag{36}$$

Notice that an η_{LCOE} value greater than 1 implies that the 1 V configuration is less efficient than the 2 V configuration.

The results of the LCOE are highly dependent on the technical and economic variables previously defined. In this sense, the following should be taken into account:

- (i) As the discount rates are country-specific [57], and the country is the same in this study, the same r can be considered (0.05%).
- (ii) The electrical power generated by the PV modules in a photovoltaic plant depends mainly on the incident solar irradiance, and PV cell temperature. In this study, these two variables are the same in the two cases of configurations studied, so the performance factor can be considered to be the same.
- (iii) As the two configurations are subject to the same meteorological conditions, the parameter d_r is considered to be the same.
- (iv) In regards to operation and maintenance costs, the recommendation of the National Renewable Energy Laboratory has been taken into account in this study [53]. Therefore, the 0.5% of the initial investment has been assumed for the operation and maintenance costs.

5. Results and discussions

According to the proposed methodology, this section shows the optimal distribution of horizontal single-axis solar trackers in a PV plant

that maximises the amount of energy captured by the PV field. This methodology is applied to a geographical location. The Granjera PV power plant (Zaragoza, Spain). Several codes have been implemented with Mathematica™ software. On the one hand, the optimisation algorithm. On the other hand, a specific Mathematica™ code calculates the direct, diffuse and reflected components of solar irradiance taking into account the effect of meteorological conditions at the site. This Mathematica™ code is based on the method proposed in [45] and takes as inputs the monthly-averaged beam and diffuse solar irradiation. These average values are obtained from the PVGIS website [58].

As in practice, the most commonly used mounting system configurations are 1 V and 2 V, these are the configurations used in this study [15]. However, the developed algorithm can easily be applied to another configuration. Therefore, in this work, the 1 V × 56, or 2 V × 56, (larger size) and 1 V × 28, or 2 V × 28, (smaller size) configurations have been considered. The width of the mounting system of the 2 V configuration is double the width of the 1 V configuration, $W_{2V} = 2 \cdot W_{1V}$.

5.1. Case study

The PV plant (Granjera PV power plant) with horizontal single-axis tracking located in Torralbilla and Langa del Castillo (Zaragoza, Spain) with latitude 41°13'48"N, longitude 1°21'00"W and altitude 884 (m) is analysed in this work. The topography of the available land considered is an irregular shape. Fig. 10 shows the location of the Granjera PV power plant, as well as the parcel \bar{P} and the rectangle R obtained with the method described in Section 3.3. The land occupied by the PV modules has an extension of 354,414 (m²).

Table 2 summarises the actual parameters of the Granjera PV power plant.

In addition, the mounting systems are separated by a North-to-South distance $e_t = 0.3$ (m) and a minimum distance from East to West $d_{\min} = 4$ (m).

5.2. Inter-row spacing design

As the Granjera PV power plant is located at a latitude of 41°13'48"N, the solar transversal incidence angle by on 21 December at 10 : 00 is $\theta_{1st} = 53.8$ (°), and according to the manufacturer $\beta_{\max} = \pm 60$ (°).

1 V Configuration

As $\theta_{1st} \leq \beta_{\max}$, d_{st} can be determined by Eq. (13) (see Fig. 5):

$$d_{st} = W_{1V} \frac{\sin^2 \theta_{1st}}{\cos \theta_{1st}} = 2.32 \text{ (m)} \tag{37}$$

And, as $d_{st} < d_{\min} = 4$ (m), case A2, e_t can be determined by Eq. (15) (see Fig. 5):

$$e_t = d_{\min} + W_{1V} \cos \beta_{\max} = 5.05 \text{ (m)} \tag{38}$$

Table 2
Actual parameters of the Granjera PV power plant.

Parameters	Value (unit)
Solar tracker	
Manufacturer	CONVERT
Model	TRJ
Type of tracking system	Horizontal single-axis tracker North–South axis alignment East–West tracking with independent rows Backtracking
Type of control	Control based on and astronomical clock algorithm
Rotation angle	Up to 120 (°) ($\beta_{max} = \pm 60$ (°))
Maximum tracking error	± 2 (°)
Maximum land slope	15% North–South; Unlimited East–West
Minimum distance over ground at maximum angle of inclination	0.4 (m)
Dimensions of the configuration 1 V × 56	61.77 × 2.11 × 2.25 (h max) (m)
Photovoltaic field area of the configuration 1 V × 56	124.59 (m ²)
Photovoltaic field length of the configuration 1 V × 56	61.24 (m)
Dimensions of the configuration 1 V × 28	30.98 × 2.11 × 2.24 (h máx) (m)
Photovoltaic field area of the configuration 1 V × 28	62.29 (m ²)
Photovoltaic field length of the configuration 1 V × 28	30.45 (m)
PV module	
Manufacturer	Longi Solar
Model	LR4-72HPH-430M
Maximum output power (STC)	430 (W)
Dimensions	2015 × 1052 × 35 (mm)
Efficiency (STC)	19.30%

2 V Configuration

As $\theta_{1st} \leq \beta_{max}$, d_{st} can be determined by Eq. (13) (see Fig. 5):

$$d_{st} = W_{2V} \frac{\sin^2 \theta_{1st}}{\cos \theta_{1st}} = 4.68 \text{ (m)} \tag{39}$$

And, as $d_{st} > d_{min} = 4$ (m), case A1, e_t can be determined by Eq. (14) (see Fig. 5):

$$e_t = d_{td} + W_{2V} \cos \beta_{td} = 7.190 \text{ (m)} \tag{40}$$

Obviously, increasing the width of the mounting system of the 2 V configuration increases the pitch, e_t . Thus, the number of mounting systems in the 2 V configuration will be smaller. This means that the initial investment cost of the installation will be reduced.

5.3. Determination of operating periods of the PV system

1 V Configuration

As $\theta_{1st} \leq \beta_{max}$, d_{st} can be determined by Eq. (13) (see Fig. 8):

$$d_{st} = W_{1V} \frac{\sin^2 \theta_{1st}}{\cos \theta_{1st}} = 2.32 \text{ (m)} \tag{41}$$

And, as $d_{st} < d_{min} = 4$ (m), A2a or A2b cases are possible.

(A2a) If the solar tracker is supposed to be in normal tracking mode:

$$d_{min} = 4 = W_{1V} \frac{\sin^2 \theta_{td}}{\cos \theta_{td}} \rightarrow \theta_{td} = 64.53^\circ \tag{42}$$

Therefore, $\theta_{td} > \beta_{max}$ is satisfied. The above supposition is not correct and the case A2b must be considered.

(A2b) As the solar tracker is not in normal tracking mode, the following equation is used:

$$d_{min} = 4 = W_{1V} \tan \theta_{td} \sin \beta_{max} \rightarrow \theta_{td} = 65.44^\circ \tag{43}$$

Therefore, $\theta_{tb} = \theta_{td} = 65.44$ (°). Using Eq. (5), $T_{b1}(n)$ and $T_{b2}(n)$ can be determined.

2 V Configuration

As $\theta_{1st} \leq \beta_{max}$, d_{st} can be determined by Eq. (13) (see Fig. 8):

$$d_{st} = W_{2V} \frac{\sin^2 \theta_{1st}}{\cos \theta_{1st}} = 4.68 \text{ (m)} \tag{44}$$

And, as $d_{st} > d_{min} = 4$ (m), this is case A1. Therefore, $\theta_{tb} = \theta_{1st} = 53.8$ (°). Using Eq. (5), $T_{b1}(n)$ and $T_{b2}(n)$ can be determined.

Fig. 11 shows the different operating periods of the solar tracker for Granjera PV power plant for the two configurations. In Fig. 11.a, 1 V configuration, you can see the 3 operating zones (backtracking mode, limited range of motion, normal tracking mode, limited range of motion, backtracking mode) mentioned above. In contrast, in Fig. 11.b, 2 V configuration, you can see the 2 operating zones (backtracking mode, normal tracking mode, backtracking mode). From the period of operation of backtracking mode, it goes directly to the normal tracking mode.

5.4. Optimal number of solar trackers

Parcel \bar{P} has an area of 354414 (m²) and is inscribed in a rectangle R of dimensions 607.569 (m) × 1139.96 (m) (see Fig. 10).

1 V Configuration

According to the manufacturer (see Table 2), the largest size, 1 V × 56 configuration has the following dimensions 61.77 × 2.11 × 2.25 (h_{max}) (m). Therefore, $L = 61.77$ (m), $W_{1V} = 2.11$ (m). In addition, the previously determined pitch has a value of $e_t = 5.05$ (m). Fig. 12.a shows 1006 mounting systems of the 1 V × 56 configuration with a PV module area of 125,338 (m²). The gaps left at the edges of the parcel (see Fig. 12.b) are then filled by the packing algorithm with the mounting systems of the smaller size, 1 V × 28 configuration (according to the manufacturer, $L = 30.98$ (m), see Table 2). In this case there are 119 mounting systems providing a PV module area of 7,412.51 (m²). The final result is shown in Fig. 12.c. An optimal area of $A_{TPV} = 132,750.51$ (m²) on a plot \bar{P} of 354,414 (m²) is obtained.

2 V Configuration

According to the manufacturer, the largest size, 2 V × 56 configuration has the following dimensions 61.77 × 4.245 × 2.25 (h_{max}) (m). Therefore, $L = 61.77$ (m), $W_{2V} = 4.245$ (m). In addition, the previously determined pitch has a value of $e_t = 7.19$ (m).

Fig. 13.a shows 703 mounting systems of the 2 V × 56 configuration with a PV module area of 175,174 (m²). The gaps left at the edges of the parcel (see Fig. 13.b) are then filled by the packing algorithm with the mounting systems of the smaller size, 2 V × 28 configuration (according to the manufacturer, $L = 30.98$ (m)). In this case there are 84 mounting systems providing a PV module area of 10,464.70 (m²). The final result is shown in Fig. 13.c. An optimal area of $A_{TPV} = 185,638.70$ (m²) on a plot \bar{P} of 354,414 (m²) is obtained.

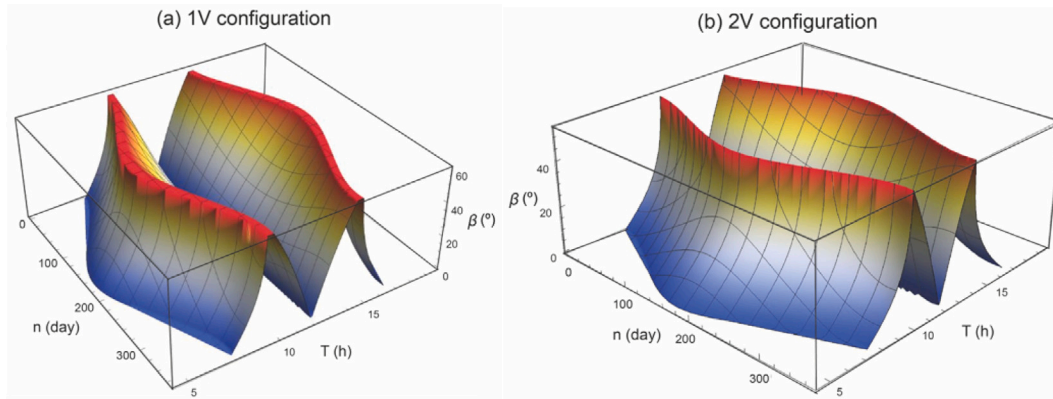


Fig. 11. Operating periods of the solar tracker for Granjera PV power plant.

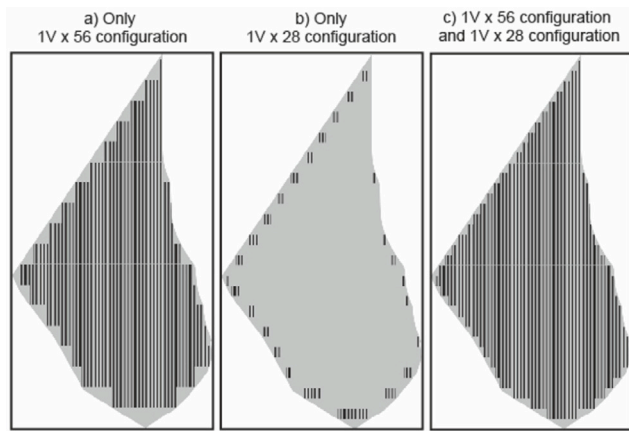


Fig. 12. Rows arrangement for the optimum distribution of PV modules for 1 V configuration.

The number of installation combinations of the mounting systems is very high, as larger and smaller size configurations have to be combined. In addition, the irregular land shape increases the complexity of this process. Therefore, performing this operation manually is very complex and time-consuming. The presented algorithm obtains the optimal combination in a reasonable time. After extensive testing, the combination $m_x \times m_y = 2 \times 10$ of possible combinations is considered to be the most suitable for the dimensions $W \times L$ and is a good compromise between computational time and accuracy for correct packing. For example for the 1 V configuration, the algorithm running time is around 5 (min) on a personal computer (Intel Core, i5–1035G1 CPU, 1.00 GHz).

On the other hand, the current Granjera PV power plant has the following values: 717 mounting systems of the 1 V × 56 configuration, 54 mounting systems of the 1 V × 28 configuration, and $A_{TPV} = 92,694.7$ (m²). Therefore, using the 1 V configuration, the proposed algorithm increases the A_{TPV} by 40,055.81 (m²). Furthermore, if the 2 V configuration is used, the proposed algorithm increases the A_{TPV} by 92,944 (m²). That is, an increase of 43.21% and 100.27%, respectively. From this point of view, the 2 V configuration is the most suitable for the Granjera PV power plant.

Comparing the current 1 V configuration of Granjera PV power plant and the 1 V configuration obtained by the algorithm, it can be seen that the proposed algorithm packs a greater number of 1 V × 56 and also a greater number of 1 V × 28 configurations, as it manages

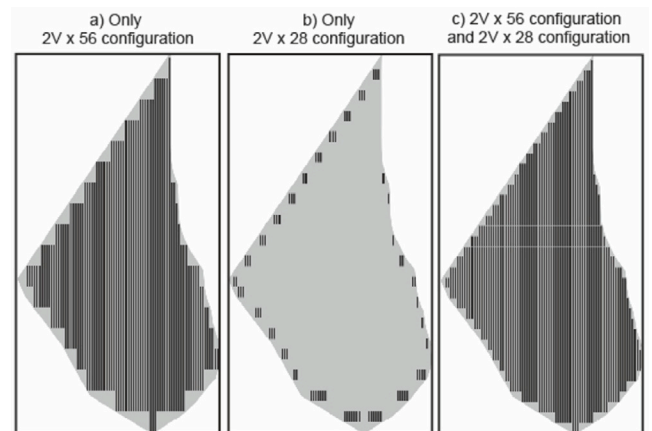


Fig. 13. Rows arrangement for the optimum distribution of PV modules for 2 V configuration.

to take better advantage of the irregular contour of the land. As a final result, it obtains a larger photovoltaic surface.

5.5. Effective annual energy incident on PV modules

Once A_{TPV} is determined and using Eq. (31) the effective annual energy incident on PV modules can be determined. Another parameter needed to determine the energy is the ground reflectance ρ_g . A value of 0.2 is commonly adopted if no information is available about ground surface [59].

Finally, the total energy $E_{TPV}(n)$ for each day of the year, n , can be calculated by multiplying the adjusted irradiance, $\mathbb{H}_i(n)$ and the total area A_{TPV} obtained from the packing algorithm. The results obtained with the 1 V and 2 V configuration are shown in Fig. 14. It can be observed that the maximum energy for 1 V configuration, with a value of 1187.53 (MWh) is obtained for day $n = 200$ (and not for $n = 172$). This is also true for the 2 V configuration, with a value of 1588.54 (MWh). The reader may also be surprised by the lack of symmetry in Fig. 14. This is because, as mentioned above, the adjusted horizontal irradiances ($\mathbb{I}_{bh}, \mathbb{I}_{dh}$) have been calculated using a method that incorporates the meteorological conditions of each location [45], and not the classical theoretical models.

The proposed algorithm determines that the total annual energy incident on the PV modules is 260.46 (GWh) for 1 V configuration, and

Table 3
Results of Granjera PV power plant.

	Configuration		
	Actual (1 V)	Proposed (1 V)	Proposed (2 V)
Input algorithm			
Area of \mathbb{P} (m ²)	354,414	354,414	354,414
Minimum distance between rows of trackers (d_{min}) (m)	4.00	4.00	4.00
Longitudinal installation distance (e_l) (m)	0.30	0.30	0.30
Limited range of motion (β_{max}) (°)	±60	±60	±60
Minimum distance on the ground (e_s) (m)	0.40	0.40	0.40
Orientation	North–South axis	North–South axis	North–South axis
PV module model	LR4-72HPH-430M	LR4-72HPH-430M	LR4-72HPH-430M
Mounting system configuration	1 V	1 V	2 V
Number of PV modules/mounting system	56 or 28	56 or 28	112 or 56
Output algorithm			
Number of total PV modules	41,664	59,668	83,440
Number of larger size configuration (x56)	717	1006	703
Number of smaller size configuration (x28)	54	119	84
Pitch (e_l) (m)	6	5.05	7.19
Annual solar irradiation (GWh)	181.88	260.46	347.73

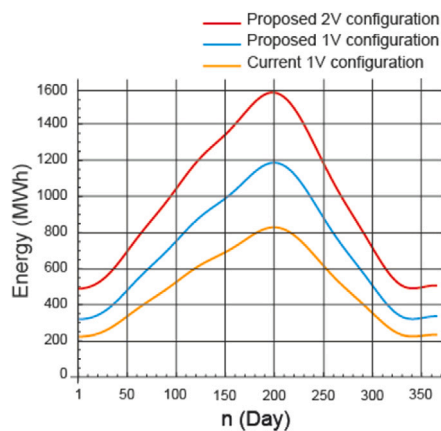


Fig. 14. The total energy $E_{TPV}(n)$.

347.73 (GWh) for 2 V configuration. In contrast, with the current distribution of the PV modules in Granjera PV power plant, an energy of 181.88 (GWh) is obtained. Therefore, the proposed algorithm increases the energy by 43.21% to 91.18%, respectively. From this point of view, the 2 V configuration is the most suitable for the Granjera PV power plant.

Based on the proposed methodology, Table 3 summarises the results for the Granjera PV power plant.

In relation to the results obtained, the following conclusions are suggested:

- (i) A 2 V configuration produces the most annual energy. Although this configuration has the greatest W , and therefore a higher pitch to avoid shading between PV modules, the 2 V configuration has twice as many PV modules as the 1 V configuration, so the equivalent pitch is lower. Therefore, using the 2 V configuration results in the highest amount of PV modules for the same surface area.
- (ii) The current 1 V configuration provides the worst result. The proposed algorithm packs a greater number of 1 V × 56, and makes better use of the irregular contour of the land, also increasing the number of 1 V × 28 configurations. As a final result, it obtains a larger photovoltaic surface.

Table 4
Total cost.

Element	Configuration		
	Actual (1 V)	Proposed (1 V)	Proposed (2 V)
N_{PV}	41,664	59,668	83,440
$C_{PV}(\text{€})$ [60]	199.90	199.90	199.90
$N_{MS}(\times 56)$	717	1006	703
$N_{MS}(\times 28)$	54	119	84
$C_{MS}(\text{€})(\times 56)$	4765.94	4765.94	5881.81
$C_{MS}(\text{€})(\times 28)$	2727.45	2727.45	3382.52
$N_{EM}(\times 56)$	717	1006	703
$N_{EM}(\times 28)$	54	119	84
$C_{EM}(\text{€})(\times 56)$ [60]	398	398	420
$C_{EM}(\text{€})(\times 28)$ [60]	398	398	420
$N_{CS}(\times 56)$	717	1006	703
$N_{CS}(\times 28)$	54	119	84
$C_{CS}(\text{€})(\times 56)$ [60]	177.61	177.61	177.61
$C_{CS}(\text{€})(\times 28)$ [60]	177.61	177.61	177.61
Total cost (€)	12,336,892.22	17,694,299.63	21,569,019.35

- (iii) Comparing the actual incident energy on the PV modules in the Granjera PV power plant with the results of the proposed algorithm, the energy increases by 43.21% for the 1 V configuration and by 91.18% for the 2 V configuration.

5.6. Assessment of the economic viability

Table 4 shows the costs of the parameters that have been considered as variables making up the total cost for each of the configurations that have been studied. These parameters are: (i) Output parameters of the proposed algorithm: N_{PV} , N_{MS} , N_{EM} , and N_{CS} ; (ii) Parameters provided by manufacturers: C_{PV} , C_{EM} , and C_{CS} ; and (iii) Output parameters of the structural analysis: C_{MS} . The structural analysis of the mounting system is detailed in Annex A. All costs of the mounting system, C_{MS} , are detailed in Annex D. All the cost are referred to date 05/10/2022.

In relation to the results obtained, the following conclusions are suggested:

- (i) The proposed 2 V configuration has the highest initial investment cost compared to the current 1 V configuration. Specifically, 71.17% for the 2 V × 56 configuration, and 165.21% for the 2 V × 28 configuration.
- (ii) The two PV plant scenarios obtained using the proposed algorithm have the highest initial investment cost, as they use a larger number of mounting systems and PV modules.

- (iii) The proposed 2 V configuration has an initial investment cost 74.83% higher than the current 1 V configuration, but has an annual energy increase of 91.18%.
- (iv) The proposed 1 V configuration has an initial investment cost 43.42% higher than the current 1 V configuration, but has an annual energy increase of 43.21%.
- (v) The proposed 2 V configuration has a 17.75% higher initial investment cost compared to the proposed 1 V configuration, and also has an annual energy increase of 25.09%.
- (vi) The current 1 V configuration and the proposed 1 V configuration have similar *LCOE* values.
- (vii) The *LCOE* of the PV plant have been compared, taking as baseline the 2 V configuration, by computing the ratio between the *LCOE* of the 1 V and the 2 V configurations and this one (see Eq. (36)). This comparison shows that the value of η_{LCOE} is 1.09. Therefore the PV plant with 1 V configuration is the worst one in relation to the *LCOE* value.

6. Conclusions

This study presents a methodology for estimating the optimal distribution of horizontal single-axis solar trackers in photovoltaic plants. Specifically, the methodology starts with the design of the inter-row spacing to avoid shading between modules, and the determination of the operating periods for each time of the day. Next, a packing algorithm is used to determine the optimal number of solar trackers that maximises the amount of energy absorbed by the photovoltaic modules. The packing algorithm is implemented in *Mathematica*[™] software. The packing algorithm used Geo-spatial data from satellite images to determine the *UTM* coordinates of the available land area for the installation of the photovoltaic modules. For this purpose, the *QGIS* software, an open-source geographic information system software, has been used. The irregular land shape increases the difficulty of solving the problem. Finally, the effective annual energy incident on photovoltaic modules is determined. The study incorporates the two most commonly used mounting systems in photovoltaic plants with single-axis solar trackers, 1 V configuration and 2 V configuration. Although any other configuration is supported by the packing algorithm. The assessment of the economic viability is formulated using the levelized cost of the produced electrical energy (*LCOE*). The unit cost of the mounting systems has been determined. For this purpose, codes and standards have been used for the structural analysis of these mounting systems. In the structural analysis, the weight of the structure, the weight of the photovoltaic modules, snow loads, wind loads and their combinations have been calculated. For this purpose, the AutoDesk Robot Structural Analysis software has been used. According to this study, the main advantages of the proposed methodology are as follows:

- (i) This methodology searches maximum energy generation for a given area of available land.
- (ii) The design of the row spacing always avoids shading between the photovoltaic modules, contributing to the increase of generated energy, and reducing the appearance of hot spots.
- (iii) A comprehensive study of the operating periods has been carried out, classifying them broadly into backtracking mode, limited range of motion and normal tracking mode. The factors on which they depend have been identified (site latitude, mounting system configuration, minimum distance between photovoltaic modules, photovoltaic module dimensions) and the equations defining them developed. This study makes it possible to determine the start of each operating period for each day of the year.
- (iv) This methodology uses packing algorithms to determine the optimal distribution of solar trackers. This increases the potential energy of the available land, while reducing the computational time in the design of photovoltaic plants.

- (v) The methodology answers three key questions in photovoltaic plant design: how many photovoltaic modules can be installed?, what is the optimal mounting system configuration?, what is the optimal mounting system layout?.
- (vi) The proposed methodology can be extended to any photovoltaic plant.

In this work, from a qualitative point of view, several conclusions can be drawn:

- (i) The configuration of the mounting system used has a strong influence on the amount of solar energy captured in the photovoltaic plant, the land area required for its installation, and its economic viability.
- (ii) The parameters of the mounting system, such as length and width, and the distance for maintenance have a great influence on the total area of the photovoltaic field.
- (iii) The larger the width of the mounting system, the larger the total area of the photovoltaic field.
- (iv) The cost of the mounting system is strongly influenced by the type of configuration. The larger its width, the higher the cost of the mounting system, because the size of the profiles of the purlins and pillars increases due to the wind loads.

The proposed methodology has been applied in Granjera photovoltaic power plant, located in Zaragoza, Spain (with latitude 41° 13'48"N, longitude 1°21'00"W and altitude 884 (m)). From a quantitative point of view, the conclusions obtained can be summarised:

- (i) In terms of land required for a given power output of the photovoltaic plant, the 2 V configuration uses less land than the 1 V configuration. In particular, for the same area of land available in the Granjera photovoltaic power plant, the surface area of the photovoltaic field using the 2 V configuration is 39.84% larger than if the 1 V configuration is used.
- (ii) The photovoltaic plant with 2 V configuration is the best option proposed by the packing algorithm in relation to the total energy captured by the photovoltaic plant. This fact can be extended to other photovoltaic plants. Although 2 V configuration has the greatest *W*, and therefore a higher pitch to avoid shading between photovoltaic modules, the 2 V configuration has twice as many photovoltaic modules as the 1 V configuration, so the equivalent pitch is lower.
- (iii) The proposed 2 V configuration increases the amount of energy captured by up to 91.18% in relation to the current of Granjera photovoltaic power plant.
- (iv) The proposed 1 V configuration increases the amount of energy captured by up to 43.21% in relation to the current of Granjera photovoltaic power plant.
- (v) The proposed 2 V configuration has an initial investment cost 74.83% higher than the current of Granjera photovoltaic power plant.
- (vi) The proposed 1 V configuration has an initial investment cost 43.42% higher than the current of Granjera photovoltaic power plant.
- (vii) The *LCOE* of the proposed 2 V configuration is better than that of the current 1 V configuration. *LCOE* efficiency is 1.09.

Designers of photovoltaic plants with single-axis solar tracking can use this tool to reduce calculation time and optimise results. This research group plans to apply this methodology in different parts of the world to analyse the influence of the latitude of the location on the design of this type of photovoltaic plant. Another line of future work would be the application of the proposed methodology in photovoltaic plants designed with bifacial modules. Future work also can analyse how some of the design parameters of the PV plant affect the annual solar irradiation received by the PV field. In this sense, firstly the

Table 5
Values of the different loads acting on the mounting system.

	Load	Standard	Configuration			
			1 V×56	1 V×28	2 V×56	2 V×28
Structural weight (kN/m ²)	Weight		AutoDesk Robot Structural Analysis			
Weight of the PV module (q_{PV}) (kN/m ²)	Weight		0.125	0.125	0.125	0.125
Snow load (kN/m ²)	Snow	(a)	1.26	1.26	1.26	1.26
Basic velocity pressure (q_b) (kN/m ²)	Wind	(b)	0.45	0.45	0.45	0.45
Exposure factor (C_e)	Wind	(c)	1.93	1.93	2.21	2.21
Pressure coefficient ($C_{p, pushing}$)	Wind	(d)	1.2	1.2	1.2	1.2
Pressure coefficient ($C_{p, suction}$)	Wind	(d)	-1.8	-1.8	-1.8	-1.8
Probability factor (C_{prob})	Wind	(e)	1	1	1	1
Pushing wind action ($q_{e, pushing}$) (kN/m ²)	Wind	(e)	1.04	1.04	1.20	1.20
Wind suction ($q_{e, suction}$) (kN/m ²)	Wind	(e)	1.56	1.56	1.81	1.81

- (a) Annex E of the code CTE DB-SE-AE [61].
- (b) Table D.1 CTE DB SE-AE [61].
- (c) Table D.2 CTE DB SE-AE [61].
- (d) UNE-EN 1991-1-7: 2018 [62].
- (e) CTE DB-SE-AE code [61].

Table 6
Material and geometrical properties of profiles used in 1 V × 56 configuration.

Element	Designation	Length (mm)	Thickness (mm)	Material	Unit	Total cost (€)
Central pillar	IPE 140	1190	–	S 280GD Z275	1	33.67
Pillar	C170 × 40 × 3	1190	3	S 280GD Z275	6	342.72
Shaft	140 × 4	8500	4	S 280GD Z275	2	1017.79
Shaft	140 × 4	5000	4	S 280GD Z275	1	299.25
Shaft	140 × 3	8500	3	S 280GD Z275	4	1588.82
Purlin	60 × 40 × 27 × 1.6		1.6	S 280GD Z275	58	537.31

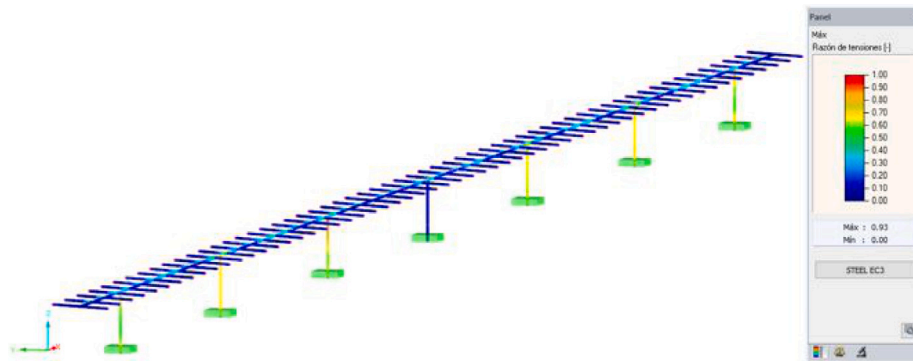


Fig. 15. Simulation obtained with the AutoDesk Robot Structural Analysis software.

influence of the maximum operating angle of the trackers, β_{max} , would be analysed. And secondly, the influence of the slope of the terrain could be studied.

CRedit authorship contribution statement

A. Barbón: Conceptualization, Methodology. **V. Carreira-Fontao:** Software, Methodology. **L. Bayón:** Conceptualization, Methodology. **C.A. Silva:** Software, Methodology, Writing – original draft.

Declaration of competing interest

The authors declare that they have no known competing financial interests or personal relationships that could have appeared to influence the work reported in this paper.

Acknowledgement

We wish to thank Gonvarri Solar Steel [15] for his contribution in this paper.

Annex A. Structural analysis of the mounting system

As indicated in the standards, in the calculation of the 1 V × 56, 1 V × 28, 2 V × 56, and 2 V × 28 configurations, the loads produced by the weight of the structure itself and of the photovoltaic modules, the environmental loads (wind and snow), and their combinations have been analysed. The model LR4-72HPH-430M manufactured by Longi Solar, with a weight of 24 (Kg) and dimensions of 2015 × 1052 × 35 (mm) has been chosen for this study.

The values of the different loads acting on the mounting system are shown in Table 5. For their calculation, the procedures indicated in the standards have been used.

In this work, the structures of the different configurations have been calculated using AutoDesk Robot Structural Analysis [63] software.

Table 7
Material and geometrical properties of profiles used in 1 V × 28 configuration.

Element	Designation	Length (mm)	Thickness (mm)	Material	Unit	Total cost (€)
Central pillar	IPE 140	1190	–	S 280GD Z275	1	33.67
Pillar	C170 × 40 × 3	1190	3	S 280GD Z275	4	228.48
Shaft	140 × 4	5000	4	S 280GD Z275	1	299.25
Shaft	140 × 3	8500	3	S 280GD Z275	2.7	1072.45
Purlin	60 × 40 × 27 × 1.6	1200	1.6	S 280GD Z275	30	277.92

Table 8
Material and geometrical properties of profiles used in 2 V × 56 configuration.

Element	Designation	Length (mm)	Thickness (mm)	Material	Unit	Total cost (€)
Central pillar	IPE 140	1900	–	S 280GD Z275	1	91.63
Pillar	C250 × 50 × 3	1900	3	S 280GD Z275	4	741.61
Shaft	140 × 4	29000	4	S 280GD Z275	1	3358.20
Purlin	60 × 40×27 × 2	3200	2	S 280GD Z275	30	808.32

Table 9
Material and geometrical properties of profiles used in 2 V × 28 configuration.

Element	Designation	Length (mm)	Thickness (mm)	Material	Unit	Total cost (€)
Central pillar	IPE 140	1900	–	S 280GD Z275	1	91.63
Pillar	C250 × 50 × 3	1900	3	S 280GD Z275	2	370.80
Shaft	140 × 4	29000	4	S 280GD Z275	1	1737
Purlin	60 × 40×27 × 2	3200	2	S 280GD Z275	16	431.10

Table 10
Costs of the control system and motor.

Element	Units for 1 V × 56	Units for 1 V × 28	Cost/un 1 V (€/un)	Units for 2 V × 56	Units for 2 V × 28	Cost/un 2 V (€/un)
Sleedrive (motor)	1	1	398	1	1	420
TCU (Tracker Control Unit)	1	1	99.05	1	1	99.05
RCU (Remote Sensor Unit)	1 unit per 200 trackers		372.33	1 unit per 200 trackers		372.33
NCU (Network Control Unit)	1 unit per 200 trackers		1776.7	1 unit per 200 trackers		1776.7
Industrial PC	1 unit per 200 trackers		1055.09	1 unit per 200 trackers		1055.09
RCU (Remote Sensor Unit)	1 unit per 200 trackers		1332	1 unit per 200 trackers		1332
Router	1 unit per 200 trackers		313.80	1 unit per 200 trackers		313.80
Scanner + GPS	1 unit per 200 trackers		929.35	1 unit per 200 trackers		929.35
Weather Station	1 unit per 200 trackers		9934.5	1 unit per 200 trackers		9934.5

Table 11
Costs of the other elements.

Element	Standard	Material	Surface treatam.	Units 1 V × 56	Units 1 V × 28	Cost 1 V (€/un)	Units 2 V × 56	Units 2 V × 28	Cost 2 V (€/un)
Joint shafts	–	–	HD G	6	4	6.10	4	2	9.40
Pillar bearing	–	–	HD G	6	4	13.90	4	2	19.90
Motor supp,	–	–	HD G	1	1	25.45	1	1	55.10
Antenna supp,	–	–	HD G	1	1	0.79	1	1	0.79
TCU supp,	–	–	HD G	2	2	4.82	2	2	4.82
NCU supp,	–	–	HD G	2	2	34.01	2	2	34.01
NCU supp,	–	–	HD G	2	2	81.63	2	2	81.63
RCU supp,	–	–	HD G	1	1	197.58	1	1	197.58
RSU supp,	–	–	HD G	1	1	36.37	1	1	36.37
Damper	–	–	–	4	2	32	2	2	32
End clamp	DIN 933	Aluminium		8	8	0.79	16	16	0.79
Clamp	DIN 933	Aluminium		108	56	1.15	104	56	1.15
Screw M16 × 40	DIN 6921 8.8	Class 8.8	HD G	72	32	0.14	52	27	0.14
Nut M16	DIN 6923 8	Class 8.8	HD G	72	32	0.02	52	27	0.02
Screw M16 × 60	DIN 6921 8.8	Class 8.8	HD G	4	4	0.15	4	4	0.15
Nut M16	DIN 6923 8	Class 8.8	HD G	4	4	0.02	4	4	0.02
Screw M10 × 55	DIN 6921 8.8 4 7	Class 8.8	HD G	24	24	0.04	16	16	0.04
Nut M10	DIN 6923 8 4 8	Class 8.8	HD G	24	24	0.01	16	16	0.01
Screw M12 × 30	DIN 6921 8.8 4 9	Class 8.8	HD G	24	24	0.08	16	16	0.08
Nut M12	DIN 6923 8	Class 8.8	HD G	24	24	0.04	16	16	0.04
Screw M16 × 30	DIN 6921 8.8	Class 8.8	HD G	116	60	0.15	60	32	0.15
Square U Bolt	SBS-04 1 7	Class 8.8	HD G	58	30	0.53	30	16	0.53
Nut M16	DIN 6923 8	Class 8.8	Stainless	116	60	0.02	60	32	0.02

Abbreviations: TCU, Tracker Control Unit; NCU, Network Control Unit; RCU, Remote Control Unit; RSU, Remote Sensor Unit; HD G, Hot-Dip Galvanising.

This programme is commonly used in structural design as it has several functions designed to simulate the behaviour of the structure under different types of loads. Fig. 15 shows one of the simulations carried out in this study using AutoDesk Robot Structural Analysis software.

Annex B. Material, geometrical properties, dimensions, and cost of the profiles used

Tables 6–9 show the material and geometric properties, dimensions, and cost of the profiles used in the fabrication of the mounting systems. These results have been obtained using AutoDesk Robot Structural Analysis software. The surface treatment of the profiles used is Hot-Dip Galvanising. These costs are referred to the date 05/10/2022.

Annex C. Control system and motor

Table 10 show the control system and motors used. These costs are referred to the date 05/10/2022.

Annex D. Auxiliary components of the mounting system

In addition to the profiles, it is also necessary to determine the auxiliary components of the mounting system such as screws, washers, nuts, clamps and end clamps. These costs are listed in Table 11. These cost are referred to date 05/10/2022.

References

- [1] United Nations (UNFCCC), Report of the conference of the parties on its twenty-first session, Paris, November to December 2015, 2022, Available from: <http://unfccc.int/resource/docs/2015/cop21/eng/10a01.pdf>. (Accessed 10 November 2022).
- [2] A. Barbón, P. Fortuny Ayuso, L. Bayón, C.A. Silva, A comparative study between racking systems for photovoltaic power systems, *Renew. Energy* 180 (2021) 424–437.
- [3] M. Ghodbane, Z. Said, A.K. Tiwari, L.S. Sundar, C. Li, B. Boumeddane, 4E (energy, exergy, economic and environmental) investigation of LFR using MXene based silicone oil nanofluids, *Sustain. Energy Technol. Assess.* 49 (2022) 101715.
- [4] A. Maheri, I. Kade Wiratama, T. Macquart, Performance of microtabs and trailing edge flaps in wind turbine power regulation: A numerical analysis using WTSim, *J. Renew. Energy Environ.* 9 (2022) 18–26.
- [5] British Petroleum, Statistical Review of World Energy, seventyth ed., 2021, <https://www.bp.com/content/dam/bp/business-sites/en/global/corporate/pdfs/energy-economics/statistical-review/bp-stats-review-2021-full-report.pdf>. (Accessed 23 November 2022).
- [6] M. Ghodbane, E. Bellos, Z. Said, B. Boumeddane, A. Khechekhoucha, M. Sheikholeslami, Z.M. Ali, Energy, financial, and environmental investigation of a direct steam production power plant driven by linear Fresnel solar reflectors, *J. Solar Energy Eng.* 143 (2021) 021008.
- [7] IRENA, Future of Solar Photovoltaic: Deployment, Investment, Technology, Grid Integration and Socio-Economic Aspects, International Renewable Energy Agency, 2019, Available from: https://irena.org/-/media/Files/IRENA/Agency/Publication/2019/Nov/IRENA_Future_of_Solar_PV_2019.pdf. (Accessed 15 November 2022).
- [8] G. Barbose, N. Darghouth, E. O'Shaughnessy, S. Forrester, *Tracking the Sun: Pricing and Design Trends for Distributed Photovoltaic Systems in the United States*, Edition 2021, Lawrence Berkeley National Laboratory, 2021.
- [9] IRENA, Solar Costs To Fall Further, Powering Global Demand, International Renewable Energy Agency, 2017, Available from: <https://www.reuters.com/article/singapore-energy-solar/solar-costs-to-fall-further-powering-global-demand-irena-idINKBN1CS13C>. (Accessed 10 November 2022).
- [10] Pvinfosights, 2022, Available from: <http://pvinsights.com/>. (Accessed 21 November 2022).
- [11] A. Barbón, C. Bayón-Cueli, L. Bayón, V. Carreira-Fontao, A methodology for an optimal design of ground-mounted photovoltaic power plants, *Appl. Energy* 314 (2022) 118881.
- [12] Z. Hua, C. Ma, J. Lian, X. Pang, W. Yang, Optimal capacity allocation of multiple solar trackers and storage capacity for utility-scale photovoltaic plants considering output characteristics and complementary demand, *Appl. Energy* 238 (2019) 721–733.
- [13] Y. Gao, J. Dong, O. Isabella, R. Santbergen, H. Tan, M. Zeman, G. Zhang, Modeling and analyses of energy performances of photovoltaic greenhouses with sun-tracking functionality, *Appl. Energy* 233 (2019) 424–442.
- [14] M. Shabani, J. Mahmoudimehr, Techno-economic role of PV tracking technology in a hybrid pv-hydroelectric standalone power system, *Appl. Energy* 212 (2018) 84–108.
- [15] Gonvarri Solar Steel, 2022, Available from: <https://www.gsolarsteel.com/>. (Accessed 25 November 2022).
- [16] S. Martín-Martínez, M. Cañas-Carretón, A. Honrubia-Escribano, E. Gómez-Lázaro, Performance evaluation of large solar photovoltaic power plants in Spain, *Energy Convers. Manage.* 183 (2019) 515–528.
- [17] A. Bahrami, C.O. Okoye, The performance and ranking pattern of PV systems incorporated with solar trackers in the northern hemisphere, *Renew. Sustain. Energy Rev.* 97 (2018) 138–151.
- [18] S.K. Saraswat, A.K. Digalwar, S.S. Yadav, G. Kumar, MCDM and GIS based modelling technique for assessment of solar and wind farm locations in India, *Renew. Energy* 169 (2021) 865–884.
- [19] P.H. Alves Verissimo, R. Antunes Campos, M. Vivian Guarnieri, J.P. Alves Verissimo, L.R. do Nascimento, R. Rütther, Area and LCOE considerations in utility-scale, single-axis tracking PV power plant topology optimization, *Sol. Energy* 211 (2020) 433–445.
- [20] M. János Maye, G. Gróf, Techno-economic optimization of grid-connected, ground-mounted photovoltaic power plants by genetic algorithm based on a comprehensive mathematical model, *Sol. Energy* 202 (2020) 210–226.
- [21] C. Bayón-Cueli, A. Barbón, A. Fernández-Conde, L. Bayón, Optimal distribution of PV modules on roofs with limited space, in: *IEEE International Conference on Environment and Electrical Engineering*, 2021, pp. 1–6.
- [22] A. Barbón, M. Ghodbane, L. Bayón, Z. Said, A general algorithm for the optimization of photovoltaic modules layout on irregular rooftop shapes, *J. Clean. Prod.* 365 (2022) 132774.
- [23] M. Tahir Patel, M. Ryyan Khan, X. Sun, M.A. Alam, A worldwide cost-based design and optimization of tilted bifacial solar farms, *Appl. Energy* 247 (2019) 467–479.
- [24] A. Aronescu, J. Appelbaum, Design optimization of photovoltaic solar fields-insight and methodology, *Renew. Sustain. Energy Rev.* 76 (2017) 882–893.
- [25] Y.M. Saint-Drenan, T. Barbier, Data-analysis and modelling of the effect of inter-row shading on the power production of photovoltaic plants, *Sol. Energy* 184 (2019) 127–147.
- [26] S. Ong, C. Campbell, P. Denholm, R. Margolis, G. Heath, Land Use Requirements for Solar Power Plants in the United States, Technical Report NREL/TP-6A20-56290, National Renewable Energy Laboratory, 2013, pp. 1–39.
- [27] N. Martín-Chivelet, Photovoltaic potential and land-use estimation methodology, *Energy* 94 (2016) 233–242.
- [28] H. Hanifi, M. Pander, B. Jaeckel, J. Schneider, A. Bakhtiari, W. Maier, A novel electrical approach to protect PV modules under various partial shading situations, *Sol. Energy* 193 (2019) 814–819.
- [29] I.H. Mahammed, A.H. Arab, S. Ibrah, Y. Bakelli, M. Khennene, S.H. Oudjana, A. Fezzani, L. Zagbba, Outdoor study of partial shading effects on different PV modules technologies, *Energy Procedia* 141 (2017) 81–85.
- [30] C. Deline, A. Dobos, S. Janzou, J. Meydbray, M.A. Donovan, A simplified model of uniform shading in large photovoltaic arrays, *Sol. Energy* 96 (2013) 274–282.
- [31] Institute for Energy Diversification and Saving, Technical Conditions for PV Installations Connected To the Grid, Spanish Government Technical Report, 2011 (in Spanish). Available from: <http://www.idae.es>. (Accessed 10 November 2022).
- [32] J.A. Duffie, W.A. Beckman, *Solar Engineering of Thermal Processes*, fourth ed., John Wiley & Sons, New York, 2013.
- [33] F.J. Casares de la Torre, M. Varo, R. López-Luque, J. Ramírez-Faz, L.M. Fernández-Ahumada, Design and analysis of a tracking/backtracking strategy for PV plants with horizontal trackers after their conversion to agrivoltaic plants, *Renew. Energy* 187 (2022) 537–550.
- [34] J. Antonanzas, R. Urraca, F.J. Martínez-de Pison, F. Antonanzas, Optimal solar tracking strategy to increase irradiance in the plane of array under cloudy conditions: A study across Europe, *Sol. Energy* 163 (2018) 122–130.
- [35] B.Y.H. Liu, R.C. Jordan, The long-term average performance of flat-plate solar energy collectors, *Sol. Energy* 7 (1963) 53–74.
- [36] J.E. Hay, Calculating solar radiation for inclined surfaces: practical approaches, *Renew. Energy* 3 (1993) 373–380.
- [37] R. Perez, P. Ineichen, R. Seals, J. Michalsky, R. Stewart, Modeling daylight availability and irradiance components from direct and global irradiance, *Sol. Energy* 44 (1990) 271–289.
- [38] E.D. Mehleri, P.L. Zervas, H. Sarimveis, J.A. Palyvos, N.C. Markatos, Determination of the optimal tilt angle and orientation for solar photovoltaic arrays, *Renew. Energy* 35 (2010) 2468–2475.
- [39] S. Makhdoomi, A. Askarzadeh, Impact of solar tracker and energy storage system on sizing of hybrid energy systems: A comparison between diesel/PV/PHS and diesel/PV/FC, *Energy* 231 (2021) 120920.
- [40] Y. Zhu, J. Liu, X. Yang, Design and performance analysis of a solar tracking system with a novel single-axis tracking structure to maximize energy collection, *Appl. Energy* 264 (2020) 114647.
- [41] R. Conceição, H.G. Silva, L. Fialho, F.M. Lopes, M. Collares-Pereira, PV system design with the effect of soiling on the optimum tilt angle, *Renew. Energy* 133 (2019) 787–796.

- [42] S. Armstrong, W.G. Hurley, A new methodology to optimise solar energy extraction under cloudy conditions, *Renew. Energy* 35 (2010) 780–787.
- [43] G. Salazar, C. Gueymard, J. Bezerra Galdino, O. Castro Vilela, Solar irradiance time series derived from high-quality measurements, satellite-based models, and reanalyses at a near-equatorial site in Brazil, *Renew. Sustain. Energy Rev.* 117 (2020) 109478.
- [44] J. Fan, B. Chen, L. Wu, F. Zhang, X. Lu, Evaluation and development of temperature-based empirical models for estimating daily global solar radiation in humid regions, *Energy* 144 (2018) 903–914.
- [45] A. Barbón, P. Fortuny Ayuso, L. Bayón, J.A. Fernández-Rubiera, Predicting beam and diffuse horizontal irradiance using Fourier expansions, *Renew. Energy* 154 (2020) 46–57.
- [46] M.A. Jallal, A. El Yassini, S. Chabaa, A. Zeroual, S. Ibnyaich, Ensemble learning algorithm-based artificial neural network for predicting solar radiation data, in: *IEEE International Conference on Decision Aid Sciences and Application, DASA, 2020*, pp. 526–531.
- [47] K. Anderson, Maximizing yield with improved single-axis backtracking on cross-axis slopes, in: *IEEE Photovoltaic Specialists Conference, PVSC 47, 2020*, pp. 1–9, Available from: <https://www.nrel.gov/docs/fy20osti/76023.pdf>. (Accessed 01 November 2022).
- [48] B. Sebbah, O. Yazidi Alaoui, M. Wahbi, M. Maâtouk, N. Ben Achhab, QGIS-Landsat indices plugin (Q-LIP): Tool for environmental indices computing using landsat data, *Environ. Model. Softw.* 137 (2021) 104972.
- [49] S. Park, A. Nielsen, R.T. Bailey, D. Trolle, K. Bieger, A QGIS-based graphical user interface for application and evaluation of SWAT-MODFLOW models, *Environ. Model. Softw.* 111 (2019) 493–497.
- [50] K. Branker, M.J.M. Pathak, J.M. Pearce, A review of solar photovoltaic levelized cost of electricity, *Renew. Sustain. Energy Rev.* 15 (2011) 4470–4482.
- [51] D.L. Talavera, E. Muñoz-Cerón, J.P. Ferrer-Rodríguez, P.J. Pérez-Higueras, Assessment of cost-competitiveness and profitability of fixed and tracking photovoltaic systems: The case of five specific sites, *Renew. Energy* 134 (2019) 902–913.
- [52] J. Mortensen, Factors Associated with Photovoltaic System Costs, National Renewable Energy Laboratory, Golden CO, 2001, pp. 1–7.
- [53] NREL, Best Practices for Operation and Maintenance of Photovoltaic and Energy Storage Systems, third ed., National Renewable Energy Laboratory, Golden, CO, 2018, Available from: <https://www.nrel.gov/docs/fy19osti/73822.pdf>. (Accessed 23 November 2022).
- [54] J. Hernandez Moro, J.M. Martinez Duart, Analytical model for solar PV and CSP electricity costs: present LCOE values and their future evolution, *Renew. Sustain. Energy Rev.* 20 (2013) 119–132.
- [55] MEPS, MEPS (International) LTD, 2018, Available from: <http://www.meps.co.uk/>. (Accessed 07 November 2022).
- [56] A. Boubault, C.K. Ho, A. Hall, T.N. Lambert, A. Ambrosini, Levelized cost of energy (LCOE) metric to characterize solar absorber coatings for the CSP industry, *Renew. Energy* 85 (2016) 472–483.
- [57] PHOTIUS 2019, 2022, Available from: https://photius.com/rankings/2019/economy/central_bank_discount_rate_2019_0.html. (Accessed 10 November 2022).
- [58] PVGIS, Joint Research Centre (JRC), 2020, Available from: http://re.jrc.ec.europa.eu/pvg_tools/en/tools.html. (Accessed 06 November 2022).
- [59] T. Muneer, *Solar Radiation and Day Light Models*, first ed., Elsevier, Oxford, 2004.
- [60] Autosolar, Technical Data, 2022, Available from: <https://autosolar.es/>. (Accessed 23 November 2022).
- [61] Spanish Technical Building Code Royal Decree 314/2006, 17 March 2006.
- [62] UNE-EN 1991-1-7: 2018, Actions on Structures, AENOR, 2018.
- [63] K. Marsh, Autodesk Robot Structural Analysis Professional 2016: Essentials, Marsh API, LLC, 2016.